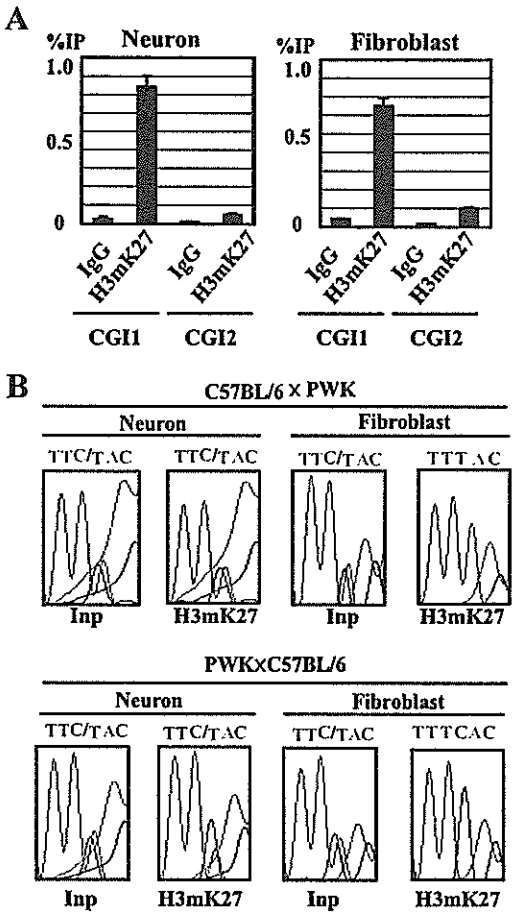

FIG. 6. Histone H3K27 methylation analysis of CGI1 and CGI2 in cultured cells. (A) Quantitative analysis of immunoprecipitated DNA by real-time PCR. The percentage of immunoprecipitation (IP) was calculated by dividing the quantitative value of precipitated DNA by that of the corresponding input DNA. Standard errors of the means are indicated by bars. (B) Allele-specific histone modifications in CGI1 by sequence chromatograms. Neurons and fibroblasts derived from F_1 hybrids (C57BL/6 × PWK; PWK × C57BL/6) were used for analysis. The single-nucleotide (C/T) polymorphism is detected in the input sample (Inp); "C" originated from the C57BL/6 allele and "T" from the PWK allele. IgG, immunoglobulin G.

Igf2r (21, 22, 23, 33, 35). Our data also showed an epigenetically unsynchronized active/silent signal between DNA methylation and histone modifications in *Grb10* (Fig. 7). In this study, we showed that the brain type transcript is expressed in neurons but not in glial cells (Fig. 2C), where both differential methylation in CGI2 and biallelic hypomethylation in CGI1 were maintained regardless of expression (Fig. 4B). The result that allele-specific DNA methylation is not sufficient to direct imprinted expression in brain cells implies that other epigenetic modifications may affect cell lineage-specific imprinting.

In our analysis of histone modifications, histone acetylation status correlated with the expression status of the major-type transcript in glial cells and fibroblasts and the brain type transcript in neurons (Fig. 7). Such histone acetylation status in *Grb10* expression is consistent with the findings that allele-specific histone acetylation was associated with allelic gene expression in the imprinted gene, *NDN* (21). Histone acetylation offers the best example of a direct link between tissue-specific gene expression and histone modifications.

Unlike that of histone acetylation, the status of histone methylation has been implicated as an early event for chromatin conformations. Methylation of histones H3K4 and H3K9 is associated with active chromatin and silent chromatin, respectively. According to our results, allele-specific H3K4 and H3K9 methylation in CGI1 and CGI2 did not correlate with allele-specific gene expression in each cultured cell. In glial cells, H3K4 in CGI2 was hypermethylated in the paternal chromosome, which was silent with no brain type transcript. It seems that H3mK4 is maintained during differentiation as an imprint mark with H3mK9 but is not related to promoter activity (28), although histone modifications in oocytes remain unknown. In CGI1, H3me2K9 and H3me3K9 were hypomethylated in both parental chromosomes independent of the expression of the major-type transcript in cultured cells. It is likely that H3K9 methylation in germ cells is maintained as a stable and heritable imprint mark but may not be secondarily acquired during development.

Then, how is maternal chromosome-specific expression of the major-type transcript regulated without differential DNA methylation in CGI1? The PcG protein Eed complex is known to be a part of a memory system that maintains repression of

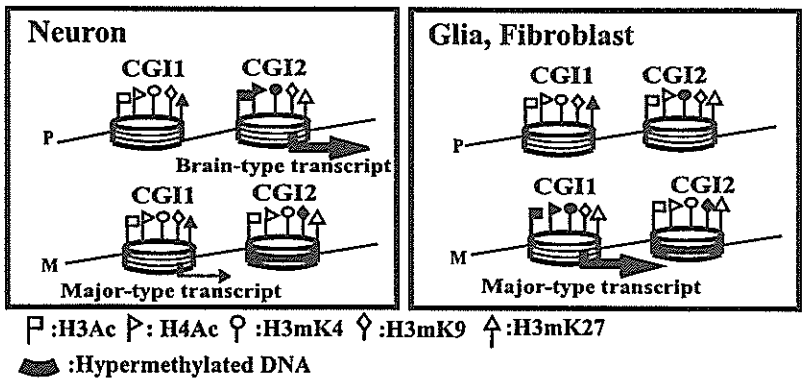

FIG. 7. Summary of epigenetic modifications across promoter regions of *Grb10*. M and P represent maternal and paternal chromosomes, respectively. Large and small arrows indicate expression levels. The nucleosome model shows DNA wrapping around a histone octamer with some histone modifications. White and black flags represent hypoacetylated/hypomethylated and hyperacetylated/hypermethylated statuses, respectively.

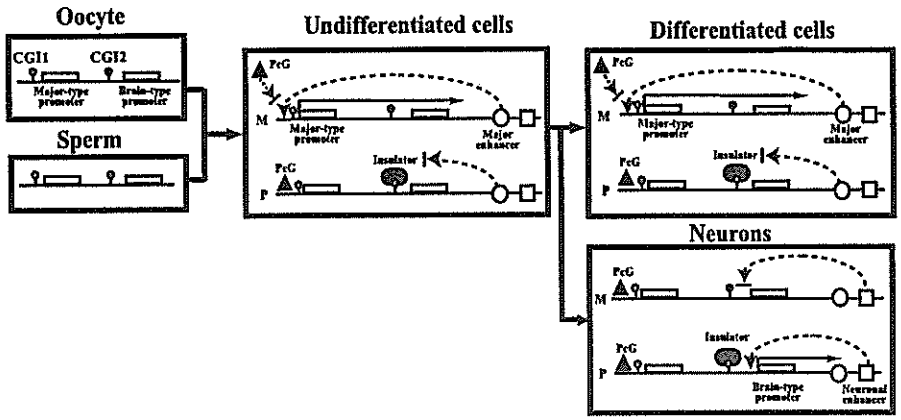

FIG. 8. Working models for tissue-specific reciprocal imprinting of *Grb10*. The previous enhancer/insulator model by Hikichi et al. was modified based on the analysis of DNA methylation and histone modifications mediated by the PcG complex containing Eed (17). Tissue-specific imprinting of *Grb10* implies neuron-specific imprinting that is different from imprinting in other undifferentiated and differentiated cells. Black and white lollipops indicate hypermethylated and hypomethylated DNA, respectively. Circles and squares indicate putative major enhancer and neuronal enhancer, respectively, which accelerate *Grb10* expression from the major-type promoter and the brain type promoter, respectively. The PcG complex containing Eed is represented by a triangle. CTCF is thought to be a putative insulator (gray oval). M, maternal; P, paternal.

the imprinted X chromosome (36) and silencing of some imprinted genes (24, 33). *Grb10* is reported to be one of the imprinted genes that are regulated by the PcG protein Eed complex. Interestingly, in $Eed^{-/-}$ embryos, the major-type transcript was biallelically expressed without major alteration of allelic DNA methylation (24). The Eed/Ezh2 PcG complex possesses histone methyltransferase activity on H3K27 (5, 8, 25) and interacts with histone deacetylases (34). Methylation of H3K27 is a repressive epigenetic mark regulated by the SET domain containing Ezh2/Eed complex (5, 8, 20, 25). In our analysis, H3mK27 was clearly precipitated in neurons and fibroblasts in CGI1 but not in CGI2 (Fig. 6A). The paternal chromosome-specific methylation of H3K27 in CGI1 was observed in fibroblasts but not in neurons (Fig. 6B). These data indicate that the Eed PcG complex can biallelically interact on CGI1 as a *trans*-acting factor in neurons but paternally in other cells. In the absence of DNA methylation in CGI1, PcG complexes may mediate a nonpermissive chromatin state for transcription, leading to repressive histone modifications. Interestingly, other genes, *Cdkn1c* and *Ascl2*, imprinting of which was reported to be regulated by Eed (24), show tissue-specific imprinting, and their imprinted expression in trophoblasts is associated with repressive histone H3K27 methylation rather than DNA methylation (22, 33).

Figure 7 shows the summary of our data. In CGI2, DNA methylation in a gametically methylated CpG island on the maternal allele was maintained throughout development. Allelic methylation of H3K4 and H3K9 associated with gametic DNA methylation was also stable as an epigenetic mark, independent of *Grb10* expression. Histone acetylation status was correlated with the expression status of the brain type transcript: histones H3 and H4 were paternally acetylated only in neurons, where the brain type transcript was paternally expressed. H3K27 was not methylated biallelically. In CGI1, biallelic DNA hypomethylation and biallelic hypomethylation of H3K9 were observed. Acetylation of histones H3 and H4 and methylation of H3K4 and H3K27 were allelically detected, corresponding to the allelic expression of the major-type transcript, although the discordance in histone modifications and expression in neurons was detected, probably depending on maturation of neurons. Methylation of H3K9 and H3K27 is thought to be a repressive chromatin marker, but it is not completely clear whether PcG-mediated silencing involves methylation of H3K9 synchronized with H3mK27 in all PcG target genes. We did not observe coexistence of H3mK27 and H3mK9 in both CGI1 and CGI2 of *Grb10*. Umlauf et al. also reported discordance between localizations of H3mK27 and H3mK9 in some imprinted genes in the *Kcnq1* domain (33). Further work should determine how histone modifications, especially methylation of H3K9 and H3K27, are coordinated or uncoordinated as epigenetic determinants in tissue-specific imprinting.

These data about epigenetic modifications analyzed at the cell level, in addition to the evidence for $Dnmt3L^{m-/-}$ and $Eed^{-/-}$ embryos, lead to a working model for tissue-specific reciprocal imprinting of *Grb10* (Fig. 8). The previous model by Hikichi et al. (17) was modified in our model based on the data of DNA methylation and repressive histone modifications mediated by the PcG complex in brain cell lineages. In undifferentiated cells, a DNA methylation-sensitive insulator, CTCF, binds to the paternal CGI2 and blocks the paternal activity of the downstream major enhancer, resulting in silent expression of the major-type transcript on the paternal allele. On the maternal allele, the major enhancer works on the major-type promoter to recruit transcription factors. In CGI1, the Eed/Ezh2 PcG complex binds on the paternal allele, whereas it competes with transcription factors on the maternal allele. The Eed/Ezh2 PcG complex methylates H3K27 and interacts with histone deacetylases, leading to silencing of the chromatin on the paternal CGI1. In $Dnmt3L^{m-/-}$ embryos, biallelic hypomethylation in CGI2 makes CTCF bind biallelically on CGI2, resulting in null expression of the major-type transcript, regardless of the PcG complex. In $Eed^{-/-}$ embryos, the silent state on the paternal CGI1 regulated by the Eed PcG complex

is released to the biallelically active state without major alteration of DNA methylation in maternal CGI2. In neurons, the other molecular mechanism of imprinting works in a promoter-specific manner, different from that in other differentiated cells. During neurogenesis, expression of *Grb10* shifts from the major-type to the brain type transcript by switching from the major-type promoter to the brain type promoter. The neuronal enhancer instead of the major enhancer may work on the brain type promoter, depending on DNA methylation in CGI2. The maternally active major-type promoter becomes silent without transcription factors, and consequently, the Eed/Ezh2 PcG complex binds to make the chromatin structure silent. This implies that the PcG complex is necessary to maintain cell-type-specific imprinting. It remains unknown how neuron-specific imprinting is regulated by DNA methylation and/or histone modifications mediated by the PcG complex, because *Dnmt3L*$^{m-/-}$ and *Eed*$^{-/-}$ embryos are lethal by E10.5 (4, 14) and E8.5 (11), respectively, just before neurogenesis.

As far as we know, this is the first report of an epigenetic analysis of cultured cells where DNA methylation and chromatin remodeling by PcG proteins establish and maintain cell-type-specific imprinting at one gene locus. Although allelic DNA methylation established in the gamete contributes primarily to tissue-specific imprinting, tissue-specific *Grb10* imprinting is directly regulated by the repressive chromatin mediated by the PcG complex during development. Our analysis of promoter-specific and cell-type-specific imprinting of *Grb10* gives an important clue for understanding the mechanism of tissue-specific imprinting.

ACKNOWLEDGMENTS

We thank F. Ishino for providing information about genomic sequences of *Grb10* promoter regions.

T.K. was supported in part by a Grant-in-Aid for Scientific Research (C) and a Grant-in-Aid on Priority Areas (Molecular Brain Science) from the Ministry of Education, Culture, Sports, Science and Technology of Japan.

REFERENCES

1. **Arnaud, P., D. Monk, M. P. Hitchins, E. Gordon, W. Dean, C. Beechey, J. Peters, W. Craigen, M. Preece, P. Stanier, G. E. Moore, and G. Kelsey.** 2003. Conserved methylation imprints in the human and mouse GRB10 genes with divergent allelic expression suggests differential reading of the same mark. Hum. Mol. Genet. **12**:1005–1019.
2. **Arnaud, P., K. Hata, M. Kaneda, E. Li, H. Sasaki, R. Feil, and G. Kelsey.** 2006. Stochastic imprinting in the progeny of Dnmt3L−/− females. Hum. Mol. Genet. **15**:589–598.
3. **Bantignies, F., and G. Cavalli.** 2006. Cellular memory and dynamic regulation of Polycomb group proteins. Curr. Opin. Cell Biol. **18**:1–9.
4. **Bourc'his, D., G. L. Xu, C. S. Lin, B. Bollman, and T. H. Bester.** 2001. Dnmt3L and the establishment of maternal genomic imprints. Science **294**: 2536–2539.
5. **Cao, R., L. Wang, H. Wang, L. Xia, H. Erdjument-Bromage, P. Tempst, R. S. Jones, and Y. Zhang.** 2002. Role of histone H3 lysine 27 methylation in Polycomb-group silencing. Science **298**:1039–1043.
6. **Cattanach, B. M., and C. V. Beechey.** 1990. Autosomal and X-chromosome imprinting. Dev. Suppl. **1990**:63–72.
7. **Constancia, M., B. Pickard, G. Kelsey, and W. Reik.** 1988. Imprinting mechanisms. Genome Res. **8**:881–900.
8. **Czermin, B., R. Melfi, D. McCabe, V. Seitz, A. Imhof, and V. Pirrotta.** 2002. Drosophila enhancer of Zeste/ESC complexes have a histone H3 methyltransferase activity that marks chromosomal Polycomb sites. Cell **111**:185–196.
9. **Davies, W., A. R. Isles, and L. S. Wilkinson.** 2005. Imprinted gene expression in the brain. Neurosci. Biobehav. Rev. **29**:421–430.
10. **Esumi, S., N. Kakazu, Y. Taguchi, T. Hirayama, A. Sasaki, T. Hirabayashi, T. Koide, T. Kitsukawa, S. Hamada, and T. Yagi.** 2005. Monoallelic yet combinatorial expression of variable exons of the protocadherin-α gene cluster in single neurons. Nat. Genet. **37**:171–176.
11. **Faust, C., A. Schumacher, B. Holdener, and T. Magnuson.** 1995. The eed mutation disrupts anterior mesoderm production in mice. Development **121**: 273–285.
12. **Fournier, C., Y. Goto, E. Ballestar, K. Delaval, A. M. Hever, M. Esteller, and R. Feil.** 2002. Allele-specific histone lysine methylation marks regulatory regions at imprinted mouse genes. EMBO J. **21**:6560–6570.
13. **Gregory, R. I., T. E. Randall, C. A. Johnson, S. Khosla, I. Hatada, L. P. O'Neill, B. M. Turner, and R. Feil.** 2001. DNA methylation is linked to deacetylation of histone H3, but not H4, on the imprinted genes *Snrpn* and *U2af1-rs1*. Mol. Cell. Biol. **21**:5426–5436.
14. **Hata, K., M. Okano, H. Lei, and E. Li.** 2002. Dnmt3L cooperates with the Dnmt3 family of de novo DNA methyltransferases to establish maternal imprints in mice. Development **129**:1983–1993.
15. **Higashimoto, K., H. Soejima, H. Yatsuki, K. Joh, M. Uchiyama, Y. Obata, R. Ono, Y. Wang, Z. Xin, X. Zhu, S. Masuko, F. Ishino, I. Hatada, Y. Jinno, T. Iwasaka, T. Katsuki, and T. Mukai.** 2002. Characterization and imprinting status of *OBPH1/Obph1* gene: implications for an extended imprinting domain in human and mouse. Genomics **80**:575–584.
16. **Higashimoto, K., T. Urano, K. Sugiura, H. Yatsuki, K. Joh, W. Zhao, M. Iwakawa, H. Ohashi, M. Oshimura, N. Niikawa, T. Mukai, and H. Soejima.** 2003. Loss of CpG methylation is strongly correlated with loss of histone H3 lysine 9 methylation at DMR-LIT1 in patients with Beckwith-Wiedemann syndrome. Am. J. Hum. Genet. **73**:948–956.
17. **Hikichi, T., T. Kohda, T. Kaneko-Ishino, and F. Ishino.** 2003. Imprinting regulation of the murine *Meg1/Grb10* and human *GRB10* genes; roles of brain-specific promoters and mouse-specific CTCF-binding sites. Nucleic Acids Res. **31**:1398–1406.
18. **Kaneda, M., M. Okano, K. Hata, T. Sado, N. Tsujimoto, E. Li, and H. Sasaki.** 2004. Essential role for de novo DNA methyltransferase Dnmt3a in paternal and maternal imprinting. Nature **429**:900–903.
19. **Kishino, T.** 2006. Imprinting in neurons. Cytogenet. Genome Res. **113**:209–214.
20. **Kuzmichev, A., K. Nishioka, H. Erdjument-Bromage, P. Tempst, and D. Reinberg.** 2002. Histone methyltransferase activity associated with a human multiprotein complex containing the Enhancer of Zeste protein. Genes Dev. **16**:2893–2905.
21. **Lau, J. C., M. L. Hanel, and R. Wevrick.** 2004. Tissue-specific and imprinted epigenetic modifications of the human *NDN* gene. Nucleic Acids Res. **32**: 3376–3382.
22. **Lewis, A., K. Mitsuya, D. Umlauf, P. Smith, W. Dean, J. Walter, M. Higgins, R. Feil, and W. Reik.** 2004. Imprinting on distal chromosome 7 in the placenta involves repressive histone methylation independent of DNA methylation. Nat. Genet. **36**:1291–1295.
23. **Li, T., T. H. Vu, G. A. Ulaner, Y. Yang, J. F. Hu, and A. R. Hoffman.** 2004. Activating and silencing histone modifications from independent allelic switch regions in the imprinted *Gnas* gene. Hum. Mol. Genet. **13**:741–750.
24. **Mager, J., N. D. Montgomery, F. P. de Villena, and T. Magnuson.** 2003. Genome imprinting regulated by the mouse Polycomb group protein Eed. Nat. Genet. **33**:502–507.
25. **Muller, J., C. M. Hart, N. J. Francis, M. L. Vargas, A. Sengupta, B. Wild, E. L. Miller, M. B. O'Connor, R. E. Kingston, and J. A. Simon.** 2002. Histone methyltransferase activity of a Drosophila Polycomb group repressor complex. Cell **111**:197–208.
26. **Nakagawachi, T., H. Soejima, T. Urano, W. Zhao, K. Higashimoto, Y. Satoh, S. Matsukura, S. Kudo, Y. Kitajima, H. Harada, K. Furukawa, H. Matsuzaki, M. Emi, Y. Nakabeppu, K. Miyazaki, M. Sekiguchi, and T. Mukai.** 2003. Silencing effect of CpG island hypermethylation and histone modifications on O6-methylguanine-DNA methyltransferase (*MGMT*) gene expression in human cancer. Oncogene **22**:8835–8844.
27. **Pirrotta, V.** 1995. Chromatin complexes regulating gene expression in Drosophila. Curr. Opin. Genet. Dev. **5**:466–472.
28. **Rougeulle, C., P. Navarro, and P. Avner.** 2003. Promoter-restricted H3 Lys 4 di-methylation is an epigenetic mark for monoallelic expression. Hum. Mol. Genet. **12**:3343–3348.
29. **Saitoh, S., and T. Wada.** 2000. Parent-of-origin specific histone acetylation and reactivation of a key imprinted gene locus in Prader-Willi syndrome. Am. J. Hum. Genet. **66**:1958–1962.
30. **Surani, M. A., S. C. Barton, and M. L. Norris.** 1984. Development of reconstituted mouse eggs suggests imprinting of the genome during gametogenesis. Nature **308**:548–550.
31. **Tilghman, S. M.** 1999. The sins of the fathers and mothers: genomic imprinting in mammalian development. Cell **96**:185–193.
32. **Uejima, H., M. P. Lee, H. Cui, and A. P. Feinberg.** 2000. Hot-stop PCR: a simple and general assay for linear quantitation of allele ratios. Nat. Genet. **25**:375–376.
33. **Umlauf, D., Y. Goto, R. Cao, F. Cerqueira, A. Wagschal, Y. Zhang, and R. Feil.** 2004. Imprinting along the *Kcnq1* domain on mouse chromosome 7 involves repressive histone methylation and recruitment of Polycomb group complexes. Nat. Genet. **36**:1296–1300.
34. **van der Vlag, J., and A. P. Otte.** 1999. Transcriptional repression mediated by the human polycomb-group protein EED involves histone deacetylation. Nat. Genet. **23**:474–478.
35. **Vu, T. H., T. Li, and A. R. Hoffman.** 2004. Promoter-restricted histone code,

not the differentially methylated DNA regions or antisense transcripts, marks the imprinting status of *IGF2R* in human and mouse. Hum. Mol. Genet. 13:2233–2245.

36. **Wang, J., J. Mager, Y. Chen, E. Schneider, J. C. Cross, A. Nagy, and T. Magnuson.** 2001. Imprinted X inactivation maintained by a mouse Polycomb group gene. Nat. Genet. 28:371–375.
37. **Wang, Y., K. Joh, S. Masuko, H. Yatsuki, H. Soejima, A. Nabetani, C. V. Beechey, S. Okinami, and T. Mukai.** 2004. The mouse *Murr1* gene is imprinted in the adult brain, presumably due to transcriptional interference by the antisense-oriented *U2af1-rs1* gene. Mol. Cell. Biol. 124:270–279.
38. **Yamasaki, K., K. Joh, T. Ohta, H. Masuzaki, T. Ishimaru, T. Mukai, N. Niikawa, M. Ogawa, J. Wagstaff, and T. Kishino.** 2003. Neurons but not glial cells show reciprocal imprinting of sense and antisense transcripts of *Ube3a*. Hum. Mol. Genet. 12:837–847.
39. **Yamasaki, Y., T. Kayashima, H. Soejima, A. Kinoshita, K. Yoshiura, N. Matsumoto, T. Ohta, T. Urano, H. Masuzaki, T. Ishimaru, T. Mukai, N. Niikawa, and T. Kishino.** 2005. Neuron-specific relaxation of *Igf2r* imprinting is associated with neuron-specific histone modifications and lack of its antisense transcript *Air*. Hum. Mol. Genet. 14:2511–2520.
40. **Yang, Y., T. Li, T. H. Vu, G. A. Ulaner, J. F. Hu, and A. R. Hoffman.** 2003. The histone code regulating expression of the imprinted mouse *Igf2r* gene. Endocrinology 144:5658–5670.

Generation of the Novel Monoclonal Antibody Against TLS/EWS-CHOP Chimeric Oncoproteins That Is Applicable to One of the Most Sensitive Assays for Myxoid and Round Cell Liposarcomas

Kosuke Oikawa, PhD, Tsuyoshi Ishida, MD,† Tetsuo Imamura, MD,⊥ Keiichi Yoshida, MS,* Masakatsu Takanashi, PhD,§ Hiroyuki Hattori, MD,‡ Akio Ishikawa,* Koji Fujita,* Kengo Yamamoto, MD,‡ Jun Matsubayashi, MD,¶ Masahiko Kuroda, MD,* and Kiyoshi Mukai, MD¶*

Abstract: The fusion oncoproteins, TLS-CHOP and EWS-CHOP, are characteristic markers for myxoid and round cell liposarcomas (MLS/RCLS). Especially, the peptide sequence of 26 amino acids corresponding to the normally untranslated *CHOP* exon 2 and parts of exon 3 (5′-UTR) is a unique structure for these chimeric proteins. In this report, we have generated monoclonal antibodies against the unique peptide sequence of TLS/EWS-CHOP oncoproteins. These antibodies reacted with TLS-CHOP fusion protein, but not reacted with normal TLS and CHOP proteins by Western blot analysis. In addition, one of the antibodies also recognized the chimeric oncoprotein in archival paraffin-embedded tissue samples of MLS/RCLS. The oncoprotein was detectable by the antibody even in the paraffin-embedded tissue samples whose mRNAs were too degraded to be detected by a nested reverse transcription-polymerase chain reaction-based assay. Thus, the molecular assay using the novel antibody is expected to be one of the most sensitive diagnostic assays for MLS/RCLS.

Key Words: myxoid liposarcoma, round cell liposarcoma, TLS-CHOP, monoclonal antibody, immunohistochemistry

(*Am J Surg Pathol* 2006;30:351–356)

All of known human myxoid and round cell liposarcomas (MLS/RCLS) are associated with chromosomal translocations.[1,8] These chromosomal translocations lead to gene fusions that encode chimeric oncoproteins consisting of an N terminus contributed by one of two related genes, *TLS* (also known as *FUS*) or *EWS*, and a C terminus contributed by the *CHOP* (also called *GADD153*) gene.[3,16,19] Both components of the resulting fusion oncoproteins are important to its transforming activity.[10,20]

These *TLS/EWS* and *CHOP* gene fusions are useful for the precise diagnosis of MLS/RCLS.[1,4,6,8,15] Various techniques, including conventional cytogenetics, Southern blotting , fluorescent in situ hybridization, and reverse transcription-polymerase chain reaction (RT-PCR), have been used to identify these lesions.[12] Especially, RT-PCR is the most widely used approach because of its specificity and sensitivity for detection of the fusion gene transcripts. It is easy in general to amplify the cDNA fragment derived from the fusion gene transcripts in fresh or snap-frozen tissue samples. Amplification of cDNA fragments from RNAs in formalin-fixed, paraffin-embedded tissue samples is, however, sometimes terribly difficult because RNAs in these tissue samples are often shortened by their degradation. Furthermore, TLS/EWS-CHOP chimeric genes have structural diversity, and we have to carefully choose the primer combination for RT-PCR to detect the chimeric genes.

In this report, we have generated novel monoclonal antibodies specific for TLS/EWS-CHOP oncoproteins. Immunohistochemical analysis using one of the antibodies was more sensitive than the nested RT-PCR for detection of the *TLS-CHOP* transcripts or its gene products in paraffin-embedded tissue samples. Thus, we expect that the antibody has a great advantage for molecular diagnosis of MLS/RCLS.

MATERIALS AND METHODS

Antibody Preparation and Western Blotting

To generate monoclonal antibodies specific for TLS-CHOP chimeric protein, we synthesized an oligopeptide (FKKEVYLHTSPHLKADVLFQTDPTAE) corresponding to the amino acids 268 to 293 of TLS-CHOP (type I)

From the *Departments of Pathology, ‡Orthopedic Surgery, and ¶Diagnostic Pathology, Tokyo Medical University, Tokyo, Japan; †Department of Pathology, Kanto Medical Center NTT-EC, Tokyo, Japan; §National Research Institute for Child Health and Development, Tokyo, Japan; and ⊥Department of Surgical Pathology, Faculty of Medicine, Teikyo University, Tokyo, Japan.

Supported in part by Grants-in-Aid from the Ministry of Education, Culture, Sports, Science and Technology of Japan, the Ministry of Health, Labour and Welfare of Japan, and Japan Health Sciences Foundation.

Reprints: Masahiko Kuroda, MD, Department of Pathology, Tokyo Medical University, 6-1-1 Shinjuku, Shinjuku-ku, Tokyo, 160-8402, Japan (e-mail: kuroda@tokyo-med.ac.jp).

fusion protein. The region is specifically translated from the normally untranslated exon 2 and parts of exon 3 of *CHOP* when *TLS* and *CHOP* are formed the chimeric oncogene. We then immunized mice against the oligopeptide. Spleen cells of an immunized mouse were fused with P3UI mouse myeloma cells as described previously.[7] Of the 159 hybrids generated, two clones showed exclusive reactivity with TLS-CHOP by ELISA. Immunoblot analyses were performed as previously described.[13] Anti-FUS/TLS (H-76) rabbit polyclonal antibody (Santa Cruz Biotechnology, Santa Cruz, CA; sc-25540) and anti-GADD153 (B-3) mouse monoclonal antibody (Santa Cruz; sc-7351) were purchased. The anti-TLS-CHOP monoclonal antibodies were used at a dilution of 1:2500, and antibodies against TLS and CHOP (GADD153) were used at a dilution of 1:200.

Cell Culture, Chemicals, and Vector Transfection

NIH 3T3 cells were obtained from ATCC and were grown as previously described.[14] Tunicamycin (Sigma) was prepared in dimethyl sulfoxide (DMSO) and used at 2 μg/mL for 8 hours.

To create an expression vector encoding *TLS-CHOP*, cDNA fragment containing the complete coding region of *TLS-CHOP* (type 1) was amplified by PCR using the primers 5′-CGGACATGGCCTCAAACG-3′ and 5′-TGTTCATGCTTGGTGCAG-3′, and inserted into the mammalian expression vector, pcDNA3.1(−) (Invitrogen). NIH3T3 cells were then transfected with the TLS-CHOP expression vector using Lipofectamine 2000 reagent (Invitrogen) and incubated for 24 hours.

Tumor Samples

Tissue samples were fixed in 20% formalin, embedded in paraffin, and stained with hematoxylin and eosin. The tumor samples used in this study were as follows: 16 myxoid liposarcomas (MLS), 5 mixed-type liposarcomas (myxoid with round cell areas) (MLS+RCLS), 2 round cell liposarcomas (RCLS), 2 well-differentiated liposarcomas (WD-LS), 2 pleomorphic liposarcomas (P-LS), 4 myxoid type malignant fibrous histiocytomas (MFH m-type), 4 storiform-pleomorphic type malignant fibrous histiocytomas (MFH s-p type), 2 leiomyosarcomas (LMS), 1 embryonal rhabdomyosarcoma (E-RMS), 2 monophasic fibrous-type synovial sarcomas (SS mf-type), 2 malignant peripheral nerve sheath tumors (MPNST), and 4 Ewing's sarcoma/primitive neuroectodermal tumors (PNET) (Tables 1, 2). All of these tumor samples were diagnosed by detailed histopathologic observation.

RNA Isolation, RT-PCR, and Immunohistochemical Analysis

Total RNA from formalin-fixed, paraffin-embedded tumor samples was extracted using ISOGEN PB Kit (Nippon gene, Tokyo, Japan). First-strand cDNA synthesis was performed as previously described.[9] We then performed nested PCR as described.[4] An aliquot of the second PCR product was fractionated by electrophoresis on a 2% agarose gel and stained with ethidium bromide. The quality of tumor RNAs was assessed by amplification of a 247-basepair portion of the ubiquitously expressed phosphoglycerate kinase (PGK) transcript as described.[2]

TABLE 1. Clinical and Molecular Findings of Myxoid and Round Cell Liposarcoma in This Study

Case	Location	Age(yr)/Sex	Histology	Tumor size (cm)	PCR		IHC
					TLS-CHOP	*PGK*	TLS/EWS-CHOP
1	rt thigh	76/F	MLS	5 × 2.5 × 1	−	−	+
2	rt lower leg	35/M	MLS+RCLS	13 × 5 × 5	type 2	+	+
3	lt thigh	50/M	MLS	unidentified	type 2	+	+
4	rt buttock	53/M	MLS+RCLS	17 × 11 × 9	type 2	+	+
5	rt thigh	51/M	MLS	30 × 15 × 15	−	−	+
6	lt thigh	33/M	RCLS	9.5 × 9.5 × 9.5	type 2	+	+
7	lt popliteal	68/M	MLS	10 × 10 × 10	nd	nd	+
8	lt thigh	37/F	MLS	4.5 × 4.5 × 4.5	nd	nd	+
9	lt thigh	40/F	MLS+RCLS	5.2 × 5.2 × 5.2	nd	nd	+
10	lt thigh	32/M	MLS	9 × 9 × 9	nd	nd	+
11	lt inguinal	47/F	MLS	6 × 6 × 6	nd	nd	+
12	lt popliteal	19/F	MLS	7 × 7 × 7	nd	nd	+
13	lt thigh	29/F	RCLS	3.9 × 3.9 × 3.9	nd	nd	+
14	lt arm	65/M	MLS	unidentified	nd	nd	+
15	lt thigh	80/M	MLS	19 × 19 × 19	nd	nd	+
16	retroperitoneum	59/F	MLS	unidentified	nd	nd	+
17	rt inguinal	40/F	MLS	8 × 8 × 8	nd	nd	+
18	rt thigh	55/F	MLS	12 × 12 × 12	nd	nd	+
19	rt thigh	61/M	MLS	17 × 17 × 17	nd	nd	+
20	rt thigh	34/M	MLS	11 × 11 × 11	nd	nd	+
21	back	50/M	MLS	14 × 14 × 14	nd	nd	+
22	lt inguinal	62/F	MLS+RCLS	5.5 × 5.5 × 5.5	nd	nd	−
23	lt thigh	64/F	MLS+RCLS	9 × 9 × 9	nd	nd	−

MLS, myxoid liposarcoma; RCLS, round cell liposarcoma; nd, not determined.

TABLE 2. Clinical, Histological, and Molecular Findings of Tumors in This Study Except for MLS/RCLS

Case	Location	Age(yr)/Sex	Histology	Tumor size (cm)	PCR		IHC
					TLS-CHOP	*PGK*	TLS/EWS-CHOP
24	mediastinum	20/M	PNET	5 × 4.5 × 2.5	–	+	–
25	mediastinum	24/M	PNET	unidentified	nd	nd	–
26	thigh	40/F	PNET	3 × 3 × 3	nd	nd	–
27	back	32/F	PNET	3.5 × 3.5 × 3.5	nd	nd	–
28	lt thigh	48/F	WD-LS	12 × 9.5 × 3.5	–	–	–
29	lt thigh	72/F	WD-LS	7 × 4.5 × 3.5	–	+	–
30	rt buttock	62/M	P-LS	6 × 5 × 5	–	+	–
31	retroperitoneum	46/M	P-LS	unidentified	nd	nd	–
32	rt back	82/M	MFH s-p type	15 × 9 × 3.5	–	–	–
33	rt thigh	77/F	MFH m-type	11 × 6 × 1	–	+	–
34	lt knee	69/M	MFH s-p type	2.8 × 2.8 × 2.8	nd	nd	–
35	rt thigh	62/F	MFH m-type	5 × 5 × 5	nd	nd	–
36	rt arm	85/F	MFH s-p type	unidentified	nd	nd	–
37	lt lower leg	46/M	MFH m-type	6 × 6 × 6	nd	nd	–
38	lt thigh	49/M	MFH s-p type	21 × 21 × 21	nd	nd	–
39	lt thigh	78/M	MFH m-type	9 × 9 × 9	nd	nd	–
40	uterus	51/F	LMS	9.5 × 9.5 × 9.5	nd	nd	–
41	pelvic cavity	74/M	LMS	13 × 13 × 13	nd	nd	–
42	left foot	48/F	E-RMS	10.5 × 10.5	nd	nd	–
43	forearm	26/F	SS mf-type	unidentified	nd	nd	–
44	thigh	46/F	SS mf-type	13 × 13 × 13	nd	nd	–
45	cheek	46/M	MPNST	3.3 × 3.3 × 3.3	nd	nd	–
46	shoulder	11/M	MPNST	26 × 26 × 26	nd	nd	–

PNET, Ewing's sarcoma/primitive neuroectodermal tumor; WD-IPS, well-differentiated liposarcoma; MFH m-type, myxoid type of malignant fibrous histiocytoma; MFH s-p type, storiform-pleomorphic type of malignant fibrous histiocytoma; LMS, leiomyosarcoma; E-RMS, embryonal rhabdomyosarcoma; SS mf-type, monophasic fibrous type synovial sarcoma; MPNST, malignant peripheral nerve sheath tumor; nd, not determined.

Standard indirect immunoperoxidase procedures were used for immunohistochemistry (LSAB2 Kit, DakoCytomation, Kyoto, Japan). After microwave pretreatment for antigen retrieval, an anti-TLS-CHOP monoclonal antibody was applied at a dilution of 1:800. Diaminobenzidine was used as the chromogen.

RESULTS

Generation of Anti-TLS/EWS-CHOP Antibodies

To generate monoclonal antibodies specific for TLS/EWS-CHOP oncoproteins, we selected the 26-amino acid oligopeptide from TLS/EWS-CHOP chimeric proteins that corresponds to the normally untranslated *CHOP* exon 2 and parts of exon 3 (5′-UTR) as the antigen (Fig. 1A). We then obtained two clones of anti-TLS/EWS-CHOP monoclonal antibodies. To confirm the specificity of these antibodies, we performed Western blot analysis with total cell lysates from NIH3T3 cells transfected with a TLS-CHOP expression vector or treated with Tunicamycin. Tunicamycin treatment induces CHOP expression.[21] As shown in Figure 1B, anti-TLS/EWS-CHOP antibodies reacted with TLS-CHOP oncoprotein but not with both normal TLS and CHOP proteins (Fig. 1B). Normal TLS and CHOP signals were shown with anti-TLS and anti-CHOP antibodies, respectively. These data indicated that the anti-TLS/EWS-CHOP antibodies specifically recognized TLS-CHOP fusion oncoprotein.

Detection of *TLS-CHOP* Fusion Transcripts in Myxoid and Round Cell Liposarcomas in Paraffin-Embedded Tissues

Our final goal of this study is to establish the most reliable and usable molecular assay for diagnosis of MLS/RCLS. Previously, Hisaoka et al reported that a nested RT-PCR-based assay could be applied to paraffin-embedded tissues to detect the *TLS-CHOP* gene transcripts as a diagnostic aid for MLS/RCLS.[4] Thus, we first examined paraffin-embedded sarcoma tissue samples obtained in this study by the nested RT-PCR-based assay. Because RNAs were not obtained from many tissue samples available in this study, we examined *TLS-CHOP* expression in only 12 cases. We also assayed *PGK* transcripts in the samples to assess the quality of their mRNAs because the *PGK* gene is ubiquitously expressed. We detected *TLS-CHOP* transcripts in 4 (67%) of 6 paraffin-embedded samples of MLS/RCLS (Table 1). The nucleotide sequences of the nested RT-PCR products were confirmed by sequence analysis. We did not identify the *PGK* gene products in the other two MLS/RCLS samples without detectable *TLS-CHOP* transcripts, suggesting that the quality of the mRNAs were insufficient for the nested RT-PCR. We did not detect *TLS-CHOP* transcripts in the tumor tissue samples except for MLS/RCLS, although *PGK* transcripts were detected in all of these tumor samples except for one myxoid variant of malignant fibrous histiocytoma (MFH) and one well-differentiated liposarcoma (WD-LS) (Table 2).

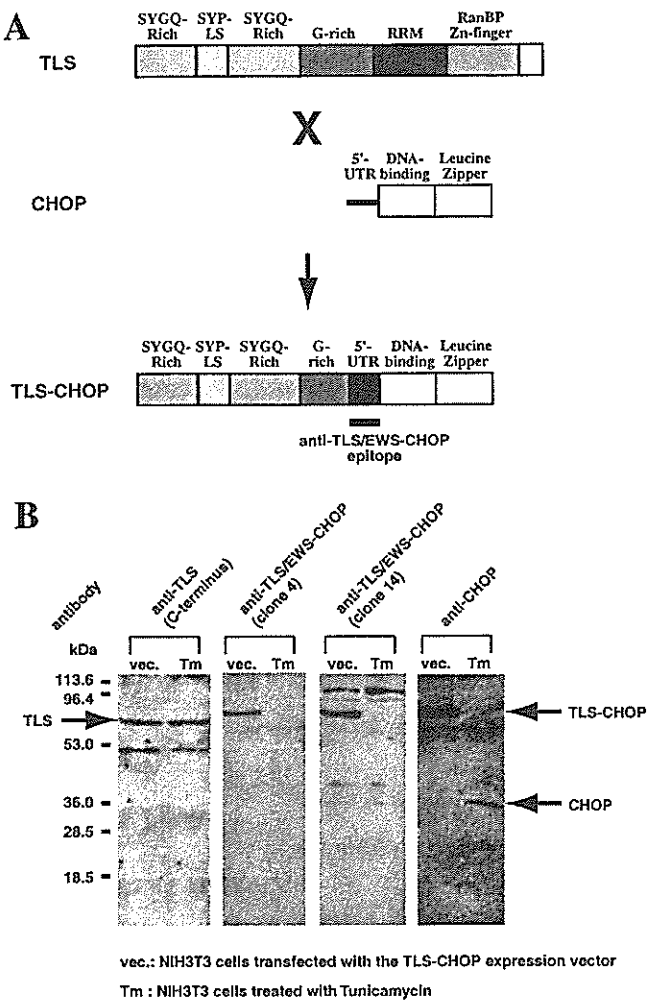

FIGURE 1. Specification of the novel anti TLS/EWS-CHOP antibodies. A, Schematic structures of TLS, CHOP, and TLS-CHOP proteins. Fusion of TLS with CHOP results in a chimeric protein where the C-terminus domains of TLS are replaced by CHOP. The peptide sequence corresponding to the normally untranslated region (5'-UTR) is expressed in the fusion protein. The recognition site of the novel monoclonal antibodies is indicated as "anti-TLS/EWS-CHOP epitope." B, Western blot analysis of TLS-CHOP protein with the total extracts from NIH3T3 cells transfected with TLS-CHOP expression vector (vec) and NIH3T3 cells expressing CHOP induced by Tunicamycin treatment (Tm) using the novel anti TLS/EWS-CHOP monoclonal antibodies. Signals of TLS and CHOP proteins were also shown by Western blot analysis using the anti-TLS (C-terminus) polyclonal antibody and the anti-CHOP monoclonal antibody, respectively.

Detection of TLS/EWS-CHOP Fusion Protein by Immunohistochemistry

We next examined whether the newly generated anti-TLS/EWS-CHOP monoclonal antibodies recognize TLS/EWS-CHOP fusion proteins in paraffin-embedded MLS/RCLS tissue samples or not. We performed immunohistochemical analysis using one of the antibodies, anti-TLS/EWS-CHOP antibody (clone 14), and observed nuclear staining of tumor cells in almost all cases (21 of 23 cases; 91%) of MLS/RCLS containing the samples without detectable TLS-CHOP transcripts by the nested RT-PCR (Table 1; Fig. 2A–F). The antibody reacted with tumor cells. Neither normal adipocytes nor endothelial cells of blood vessel were recognized. On the other hand, we did not detect positive nuclear staining in MFH, WD-LS, P-LS, LMS, E-RMS, SS, MPNST, and PNET samples (Table 2; Fig. 2G–J). Slight background staining was also observed in cytoplasm of muscle tissue cells (data not shown). However, it was easy to distinguish the background staining from TLS/EWS-CHOP-positive staining because of their localizations. This background signal may correspond to the 100-kDa protein reacted with the antibody (clone 14) by Western blot analysis (Fig. 1B). TLS/EWS-CHOP antibody (clone 4) failed to detect TLS-CHOP in all cases of paraffin-embedded tissue samples.

DISCUSSION

The *TLS/EWS-CHOP* fusion genes are characteristic for MLS/RCLS. Most of human MLS/RCLS are associated with the specific chromosomal translocations that led to these gene fusions.[8] Thus, these chimeric genes or their gene products are expected to be useful diagnostic molecular markers for diagnosis of MLS/RCLS. There are, however, several structural variants of the *TLS/EWS-CHOP* fusion genes as shown in Fig. 3.[5] In this report, we have generated novel monoclonal antibodies, anti-TLS/EWS-CHOP antibodies (clones 4 and 14), against the normally untranslated *CHOP* exon 2 and parts of exon 3 (5'-UTR). The antibodies are expected to recognize every variant form of TLS/EWS-CHOP except for TLS-CHOP type 4 (Fig. 3). In addition, the anti-TLS/EWS-CHOP antibody (clone 14) is able to detect the fusion oncoproteins even in paraffin-embedded tissue samples of MLS/RCLS (Fig. 2B, D, F). Thus, the non-positive-stained cases (case nos. 22 and 23) of MLS/RCLS by immunohistochemistry using the antibody (clone 14) (Table 1) may have TLS-CHOP type 4, although their subtypes were not confirmed because their RNAs were unavailable. The undetectable TLS-CHOP type 4 is, however, only a small portion (2.5%) of the whole MLS/RCLS cases (Table 3).[4–6,8,16,17] Therefore, the novel anti-TLS/EWS-CHOP antibody (clone 14) may become a strong tool for diagnosis of MLS/RCLS.

TLS/EWS-CHOP play important role in the oncogenesis of MLS/RCLS.[9,11] Although the mechanism of oncogenesis by TLS/EWS-CHOP is not fully understood, the chimeric oncoproteins are thought to induce unscheduled expression of genes associated with adipocyte differentiation as a transcription factor.[11] However, we detected obvious positive staining for TLS-CHOP

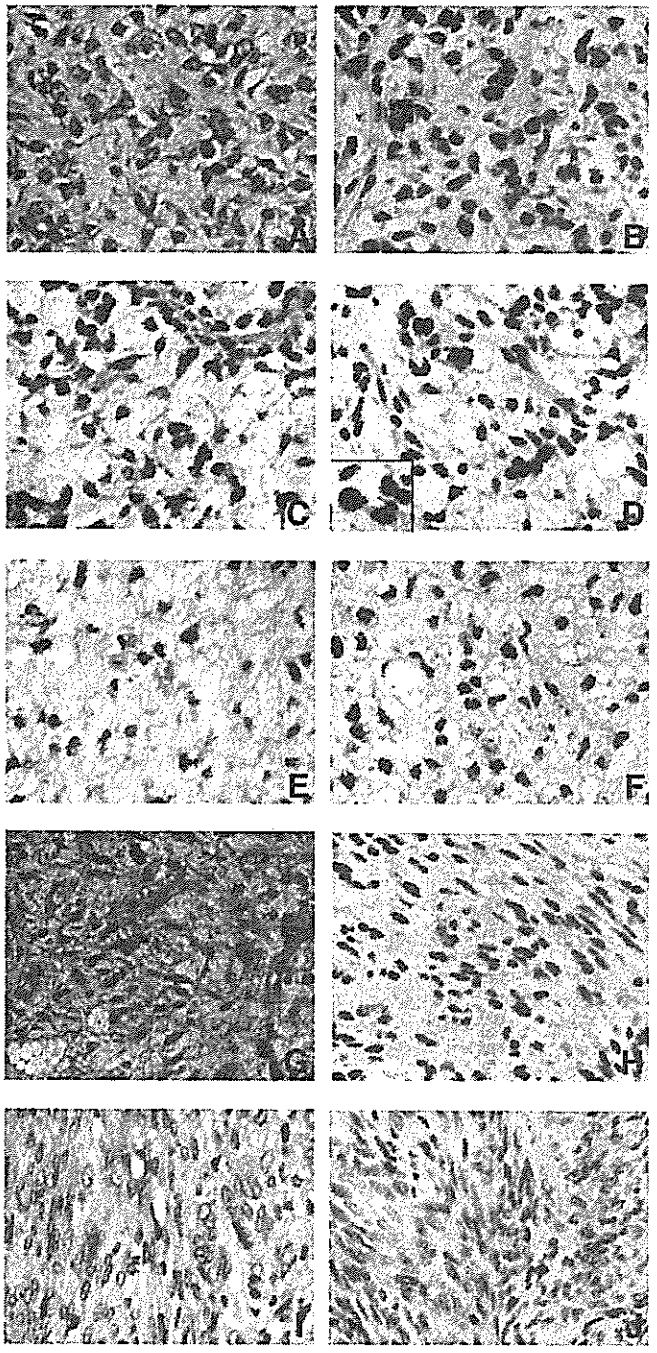

FIGURE 2. Immunohistochemical analysis using anti TLS/EWS-CHOP antibody (clone 14) (original magnification ×400). A, C, E, G, and I, Hematoxylin and eosin staining. B, D, F, H, and J, TLS/EWS-CHOP immunostaining. A, B, MLS+RCLS (case no. 2) shows uniform round cell proliferation and nuclear immunostaining for TLS-CHOP in tumor cells. MLS (case no. 3) (C, D) and MLS (case no. 1) (E, F) show proliferation of lipoblasts with plexiform capillary network and myxoid material, and nuclear immunostaining for TLS-CHOP in tumor cells. D (inset), TLS-CHOP expression in mitotic cells. P-LS (case no. 9) (G, H) and LMS (case no. 41) (I, J) show proliferation of undifferentiated cells, and no positive immunostaining.

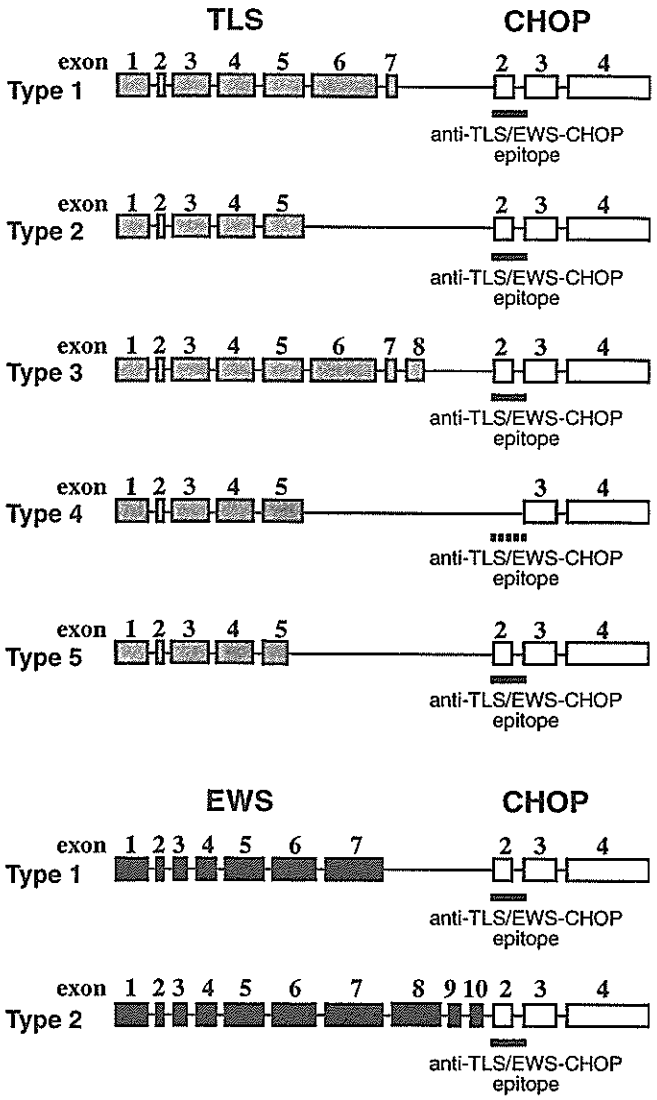

FIGURE 3. Structures of *TLS-CHOP* and *EWS-CHOP* fusion genes. The structure of each fusion gene is schematically represented. Gray, black, and open boxes represent exons of the *TLS*, *EWS*, and *CHOP* genes, respectively. The antibody recognition site is indicated as "anti TLS/EWS-CHOP epitope." Only *TLS-CHOP* type 4 does not have the epitope site.

protein even in cells during mitosis (Fig. 2D). This observation suggests that the chimeric oncoproteins may affect some mitotic mechanisms, such as chromosome segregation, and induce chromosome instability. Elucidation of this hypothesis requires further studies, and we expect that the novel anti-TLS-CHOP antibody may be helpful to reveal the mechanism of MLS/RCLS oncogenesis. Nevertheless, we now introduce the TLS/EWS-CHOP specific antibody (clone 14) as one of the best tools for diagnostic assays of MLS/RCLS.

TABLE 3. Variant form of *TLS-CHOP* and *EWS-CHOP*

		Panagopoulos et al.[17]	Knight et al.[6]	Kuroda et al.[8]	Panagopoulos et al.[16]	Hisaoka et al.[4]	Hosaka et al.[5]	This study	Total (cases)	Rate (%)
TLS-CHOP	Type 1	6		3		9	5		23	28.0
	Type 2	10	10	3		13	8	4	48	58.5
	Type 3			1			1		2	2.4
	Type 4						2		2	2.4
	Type 5						1		1	1.2
EWS-CHOP	Type 1				2		2		4	4.9
	Type 2						2		2	2.4
		16	10	7	2	22	21	4	82	100

REFERENCES

1. Antonescu CR, Elahi A, Humphrey M, et al. Specificity of TLS-CHOP rearrangement for classic myxoid/round cell liposarcoma: absence in predominantly myxoid well-differentiated liposarcomas. *J Mol Diagn.* 2000;2:132–138.
2. Antonescu CR, Kawai A, Leung DH, et al. Strong association of SYT-SSX fusion type and morphologic epithelial differentiation in synovial sarcoma. *Diagn Mol Pathol.* 2000;9:1–8.
3. Crozat A, Aman P, Mandahl N, et al. Fusion of CHOP to a novel RNA-binding protein in human myxoid liposarcoma. *Nature.* 1993;363:640–644.
4. Hisaoka M, Tsuji S, Morimitsu Y, et al. Detection of TLS/FUS-CHOP fusion transcripts in myxoid and round cell liposarcomas by nested reverse transcription-polymerase chain reaction using archival paraffin-embedded tissues. *Diagn Mol Pathol.* 1998;7:96–101.
5. Hosaka T, Nakashima Y, Kusuzaki K, et al. A novel type of EWS-CHOP fusion gene in two cases of myxoid liposarcoma. *J Mol Diagn.* 2002;4:164–171.
6. Knight JC, Renwick PJ, Cin PD, et al. Translocation t(12;16)(q13;p11) in myxoid liposarcoma and round cell liposarcoma: molecular and cytogenetic analysis. *Cancer Res.* 1995;55: 24–27.
7. Kuroda M, Horiuchi H, Ono A, et al. Immunohistochemical study on the distribution of sarcoplasmic reticulum calcium ATPase in various human tissues using novel monoclonal antibodies. *Virchows Arch A Pathol Anat Histopathol.* 1992;421:527–532.
8. Kuroda M, Ishida T, Horiuchi H, et al. Chimeric TLS/FUS-CHOP gene expression and the heterogeneity of its junction in human myxoid and round cell liposarcoma. *Am J Pathol.* 1995;147: 1221–1227.
9. Kuroda M, Ishida T, Takanashi M, et al. Oncogenic transformation and inhibition of adipocytic conversion of preadipocytes by TLS/FUS-CHOP type II chimeric protein. *Am J Pathol.* 1997;151: 735–744.
10. Kuroda M, Sok J, Ron D. *The TLS-CHOP Oncogene and Human Liposarcoma.* Landes Bioscience: Georgetown TX; 1998.
11. Kuroda M, Wang X, Sok J, et al. Induction of a secreted protein by the myxoid liposarcoma oncogene. *Proc Natl Acad Sci USA.* 1999; 96:5025–5030.
12. Ladanyi M, Bridge JA. Contribution of molecular genetic data to the classification of sarcomas. *Hum Pathol.* 2000;31:532–538.
13. Oikawa K, Ohbayashi T, Mimura J, et al. Dioxin stimulates synthesis and secretion of IgE-dependent histamine-releasing factor. *Biochem Biophys Res Commun.* 2002;290:984–987.
14. Oikawa K, Ohbayashi T, Mimura J, et al. Dioxin suppresses the checkpoint protein, MAD2, by an aryl hydrocarbon receptor-independent pathway. *Cancer Res.* 2001;61:5707–5709.
15. Panagopoulos I, Aman P, Mertens F, et al. Genomic PCR detects tumor cells in peripheral blood from patients with myxoid liposarcoma. *Genes Chromosomes Cancer.* 1996;17:102–107.
16. Panagopoulos I, Hoglund M, Mertens F, et al. Fusion of the EWS and CHOP genes in myxoid liposarcoma. *Oncogene.* 1996;12: 489–494.
17. Panagopoulos I, Mandahl N, Ron D, et al. Characterization of the CHOP breakpoints and fusion transcripts in myxoid liposarcomas with the 12;16 translocation. *Cancer Res.* 1994;54:6500–6503.
18. Rabbitts TH. Chromosomal translocations in human cancer. *Nature.* 1994;372:143–149.
19. Rabbitts TH, Forster A, Larson R, et al. Fusion of the dominant negative transcription regulator CHOP with a novel gene FUS by translocation t(12;16) in malignant liposarcoma. *Nat Genet.* 1993;4:175–180.
20. Zinszner H, Albalat R, Ron D. A novel effector domain from the RNA-binding protein TLS or EWS is required for oncogenic transformation by CHOP. *Genes Dev.* 1994;8:2513–2526.
21. Zinszner H, Kuroda M, Wang X, et al. CHOP is implicated in programmed cell death in response to impaired function of the endoplasmic reticulum. *Genes Dev.* 1998;12:982–995.

Lung Cancer (2005) 50, 43–49

ELSEVIER

LUNG CANCER

www.elsevier.com/locate/lungcan

Aberrant methylation of *FBN2* in human non-small cell lung cancer

Hong Chen[a,c], Makoto Suzuki[a,d,*], Yohko Nakamura[b], Miki Ohira[b], Soichiro Ando[a], Tomohiko Iida[a,d], Takahiro Nakajima[a,d], Akira Nakagawara[b], Hideki Kimura[a]

[a] *Division of Thoracic Diseases, Chiba Cancer Center, 666-2, Nitona, Chuoh-ku, Chiba 260-8717, Japan*
[b] *Division of Biochemistry, Chiba Cancer Center, 666-2, Nitona, Chuoh-ku, Chiba 260-8717, Japan*
[c] *Department of Pulmonary Disease, The First Affiliated Hospital, Chongqing Medical University, 1 Youyi Road, Yuzhong District, Chongqing 400016, China*
[d] *Department of Thoracic Surgery, Graduate School of Medicine, Chiba University, 1-8-1 Inohana, Chuoh-ku, Chiba 260-8670, Japan*

Received 27 December 2004; received in revised form 5 April 2005; accepted 12 April 2005

KEYWORDS
FBN2;
Methylation;
Lung cancer;
Invasion;
Metastasis

Summary FBN2, a large modular extracellular matrix glycoprotein, is known to be a key component of human elastic fiber. A loss of *FBN2* expression due to promoter methylation was recently identified in pancreatic cancer. We examined *FBN2* expression by reverse transcription PCR and aberrant methylation of *FBN2* by methylation specific PCR in lung cancer cell lines. Aberrant methylation of *FBN2* was present in 55% (6 of 11) of non-small cell lung cancer (NSCLC) cell lines, but it absent in small cell lung cancer cell lines. The concordance between loss of expression and aberrant methylation of *FBN2* was 88% (14 of 16) in the cell lines. *FBN2* expression was restored after treatment with the demethylating agent, 5-aza-2′-deoxycytidine in all six cell lines tested that lacked *FBN2* expression. Among primary NSCLC, 49% (62/126) of cases had *FBN2* methylation, but only 7% (5/69) of the corresponding nonmalignant lung tissues had it. Although *FBN2* methylation was detected even in patients with early stage disease, it occurred frequently in large tumors ($p=0.022$), with nodal metastasis ($p=0.037$), or with advanced stages of NSCLC ($p=0.014$). Methylation and silencing of *FBN2* in tumor cells may play an important role in carcinogenesis, invasion, and metastasis of NSCLC.

1. Introduction

It is well known that genetic abnormalities of proto-oncogenes and tumor suppressor genes (TSGs) are frequently involved in lung cancer pathogenesis.

* Corresponding author. Tel.: +81 43 222 7171x5464; fax: +81 43 226 2172.
E-mail address: suzumako@ra2.so-net.ne.jp (M. Suzuki).

0169-5002/$ – see front matter © 2005 Elsevier Ireland Ltd. All rights reserved.
doi:10.1016/j.lungcan.2005.04.013

The mechanism for inactivation of TSGs is gradually becoming more clearly understood. Epigenetic inactivation of certain TSGs by aberrant promoter methylation is frequently observed in lung cancer and seems to play an important role in the pathogenesis of this cancer [1–4]. In addition, the study of the loss of heterozyosity (LOH) which is also involved in the carcinogenesis of lung cancer, showed that correlations between LOH on different chromosomes suggested previously unknown genetic interactions for lung cancer development [5]. So, whereas the DNA methylation of multiple genes has been studied in lung cancer [6–8], further studies of epigenetic alternation are still needed to clarify fully the biological mechanism of lung cancer.

Fibrillin 2 (FBN2), an extracellular matrix protein, is associated with elastic fibers in several tissues and is believed to serve as a ligand for alphavbeta3 integrin, the latter being a known morphogen. *FBN2* was first expressed in the mesenchyme and at the epitheliomesenchymal interface. Latter, its expression was intensified and was confined around the tracheobronchial airways. Fibrillin-2 antisense oligodeoxynucleotide can induce dysmorphogenesis of the lung explants. FBN2 plays a key role in lung development [9].

Recently, the loss of *FBN2* expression due to promoter methylation was identified in pancreatic cancer cell lines by means of high-throughput microarray analysis [10]. Of the 12 genes silenced by methylation of 5′ regions, FBN2 was methylated in about 75% of the samples, which is a much higher proportion than for the other genes. This gene maps to 5q23-q31, a locus frequently showing allelic imbalance in lung cancer, and was speculated to act as a TSG [5]. This prompted us to examine the methylation status of *FBN2* in lung cancers. We examined methylation by methylation specific PCR (MSP), and the mRNA expression of *FBN2* by reverse transcription PCR (RT-PCR), in lung cancer cell lines, and analyzed the methylation status of primary lung cancers, and then correlated this with the clinico-pathological features.

2. Materials and methods

2.1. Cell lines and clinic samples

Eleven non-small cell lung cancer (NSCLC) and five small cell lung cancer (SCLC) cell lines were used in this study. These cell lines were established and provided by Dr. Adi F. Gazdar of University of Texas (UT) Southwestern Medical Center. Cell lines having the prefix NCI were established at the National Cancer Institute, while those with the prefix HCC were established at UT Southwestern Medical Center. They were grown in RPMI-1640 medium supplemented with 5% fetal bovine serum and incubated in 5% CO_2 at 37 °C. Nonmalignant human bronchial epithelial cells (NHBEC) were cultured as reported previously [11], and normal tracheal RNA was obtained from Clontech (Palo Alto, CA).

Surgically resected specimens of 126 patients with primary lung cancer and 69 adjacent lung tissues were obtained from Chiba Cancer Center, Japan, after obtaining Institutional Review Board approval and informed consent had been granted. Samples were immediately frozen and stored at −80 °C until used. The clinical characteristics of these patients are detailed in Table 1.

2.2. RNA preparation and RT-PCR

FBN2 mRNA expression was examined by RT-PCR. Total RNA was obtained from these cell lines (NHBEC, 11 NSCLC and 5 SCLC cell lines) by the single-step method. The reverse transcription reaction was performed on 5 μg of total RNA with the SuperScript II First-Strand Synthesis using oligo(dT) primer System (Life Technologies Inc.), and aliquots of the reaction mixture were used for the subsequent PCR amplification. Expression of β-actin was used as an internal control to confirm the success of the reverse transcription reaction. The forward PCR amplification primer of *FBN2* was 5′-GGCGAGGACAGCAGGAC-3′, and the reverse primer 5′-TGATATTTGCCCACTGGAACA-3′. The forward PCR amplification primer of β-actin was 5′-CAACTGGGACGACATGGAGA-3′, and the reverse primer 5′- ACGTACATGGTGGGGTGTTG-3′. These primer sequences were identical to the human target genes as was confirmed by BLAST searches. PCR products were analyzed on 2% agarose gels stained with ethidium bromide. NHBEC and normal tracheal cells were used as normal controls for RT-PCR.

2.3. 5-Aza-2′-deoxycytidine (5-Aza-CdR) treatment

Six tumor cell lines with negative gene expression were incubated in culture medium with 1 μM of the demethylating agent 5-aza-dC (Sigma-Aldrich, St. Louis, Mo) for 6 days, with medium changes on days one, three and five. Cells were harvested and RNA was extracted at day 6.

Table 1 Clinical characteristics and *FBN2* methylation of lung cancer patients

Clinical factors	No. of cases	No. of *FBN2* methylation (%)	*p*-value[a]
Gender			
Male	73	38 (52)	NS
Female	53	24 (45)	
Age			
≤65[b]	58	25 (43)	NS
>65	68	37 (54)	
Smoke			
Never	47	20 (43)	NS
Smoker	79	42 (53)	
Histology			
Adenocarcinoma	92	49 (53)	NS[c]
Squamous cell carcinoma	30	11 (37)	
Others (ad-sq, Large)	4	2 (50)	
pT			
T1	53	20 (38)	0.022
T2, 3 4	73	42 (58)	
pN			
N0	76	32 (42)	0.037
N1, 2, 3	50	30 (60)	
pStage			
I	54	20 (37)	0.014
II, III, IV	72	42 (58)	

[a] Fisher's exact probability test.
[b] Devided into two groups by median age.
[c] Adenocarcinoma vs. squamous cell carcinoma ad-sq, adeno-squamous cell carcinoma; NS, not significant.

2.4. DNA preparation, bisulfite modification and MSP

Genomic DNA was obtained from lung cancer cell lines, cultured nonmalignant cells, primary tumors and adjacent nonmalignant tissues by digestion with proteinase K (Life Technologies, Inc.), followed by phenol/chloroform (1:1) extraction [12]. One microgram of genomic DNA was further subjected to bisulfite treatment following the protocol of the EZ DNA Methylation Kit (Zymo Research). The modified DNA was used as a template for MSP. DNA methylation patterns in the CpG island of *FBN2* were determined by the method of MSP as reported previously [10]. Primer sequences of *FBN2* for the unmethylated reaction were: 5′-TATGGGAAT -TTGTTGAGTTTTGT-3′ (sense), and 5′-AACCAACAACCCCAAACA-3′ (antisense), which amplify a 171 bp product. Primer sequences of *FBN2* for the methylated reaction were: 5′-GGGAATTCGTCGAGTTTTGC-3′ (sense), and 5′-AACCGACAACCCCGAACG-3′ (antisense), which amplify a 168 bp product. Universal Methylated DNA (Chemicon, CA) which was subjected to bisulfite treatment was used as a positive control for methylated alleles. Controls without DNA were included in each assay. Nine microlitre of each PCR product was loaded on 2% agarose gels stained with ethidium bromide. Results were confirmed by repeating the bisulfite treatment and MSP for all samples.

2.5. Statistical analysis

The differences of methylation between the two groups were analyzed by using Fisher's exact test. Survival was calculated from the date of initial diagnosis until death or the date of the last follow-up. Survival was analyzed, according to the Kaplan-Meier method, and differences in their distribution were evaluated by means of the log-rank test. A probability value of p less than 0.05 was regarded as statistically significant. All Ps are two-sided.

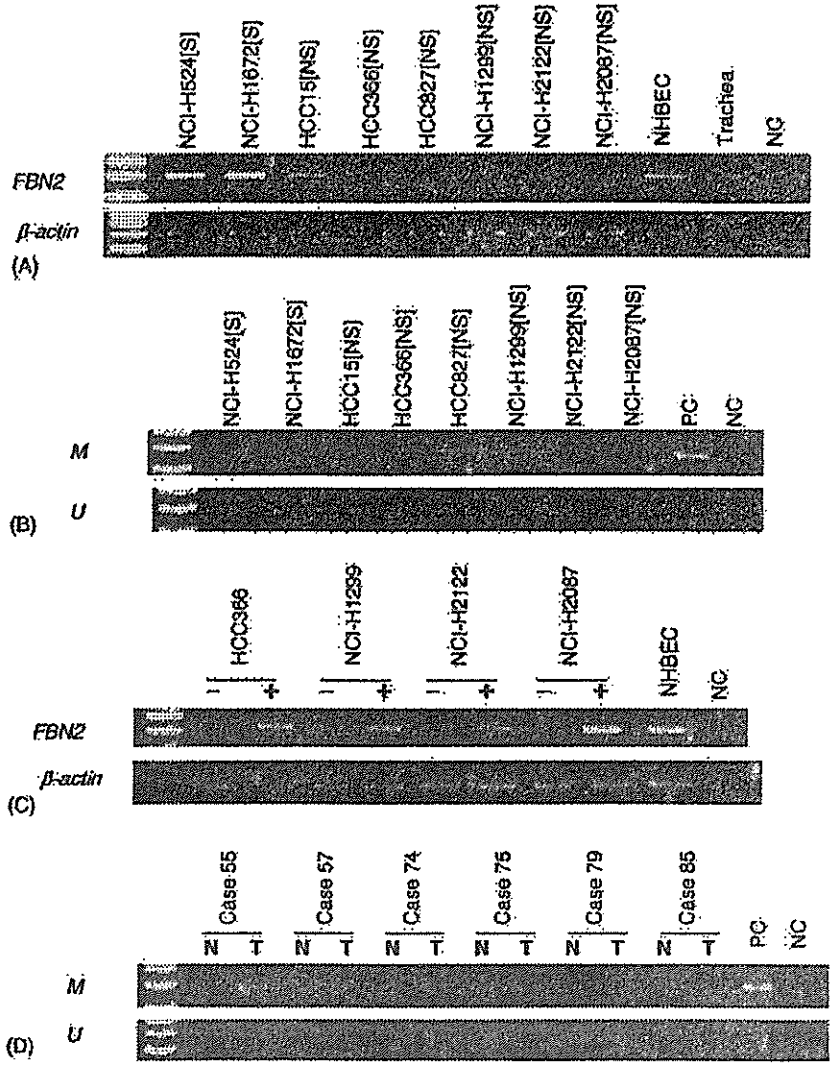

Fig. 1 (A) Representative examples of RT-PCR assay for *FBN2* RNA expression in NSCLC and SCLC cell lines. Expression of β-actin was used as a control for cDNA normalization. NHBEC and trachea were used as positive controls; NC, negative control. [NS], NSCLC; [S], SCLC. Lanes that do not show a band represent samples with loss of expression. (B) Methylation analysis of *FBN2* in cell lines. Lane U, amplified product with primers recognizing an unmethylated sequence (171-bp PCR product); Lane M, amplified product with primers recognizing a methylated sequence (168-bp PCR product). PC, positive control; NC, negative control. C, reexpression of *FBN2* after treatment with 5-Aza-2'-deoxycytidine (5-Aza-CdR). The expression of *FBN2* lost in those cell lines can be restored after treatment with 5-Aza-CdR. —, cell line without 5-Aza-CdR; +, cell line with 5-Aza-CdR; NHBEC was used as the positive control. (D), Representative examples of methylation analysis of *FBN2* in tumor specimens. N, nonmalignant lung tissue; T, tumor.

3. Results

3.1. Expression of *FBN2* in cell lines

FBN2 expression was examined by RT-PCR, and representative examples are shown in Fig. 1. Expression of *FBN2* was present in NHBEC and normal trachea. However, loss of *FBN2* expression was observed in 50% (8/16) of lung cancer cell lines, respectively, in 64% (7/11) of NSCLC cell lines, and in 20% (1/5) of SCLC cell lines.

3.2. Aberrant methylation of *FBN2* in cell lines

Detailed results of the aberrant methylation of *FBN2* in cell lines are showed in Fig. 1. Aberrant methylation was absent in NHBEC, but was observed

in 38% (6/16) of lung cancer cell lines, in 55% (6/11) of NSCLC cell lines, but in no SCLC cell lines. Only two cell lines (NCI-H524 and HCC15) demonstrated loss of expression and lack of methylation of *FBN2*. The concordance between gene expression and methylation of *FBN2* was 91% (10/11) in the NSCLC cell lines, and 80% (4/5) in the SCLC cell lines (overall concordance: 88%).

3.3. 5-Aza-CdR treatment

To confirm that the promoter methylation was responsible for silencing the *FBN2* expression, we treated methylated NSCLC cell lines (HCC366, HCC827, NCI-H1299, NCI-H2087, NCI-H2122, and NCI-H2887) that showed loss of *FBN2* expression with the demethylating agent 5-Aza-CdR. *FBN2* expression was restored after the treatment in all six cell lines tested (Fig. 1).

3.4. Aberrant methylation of *FBN2* in primary lung cancers

FBN2 methylation of primary tumors and corresponding nonmalignant tissues are detailed in Table 1 and representative samples are illustrated in Fig. 1. *FBN2* methylation was observed in 49% (62/126) of tumors, but in only 7% (5/69) of corresponding nonmalignant tissues. Methylation was tumor-specific when compared with that of corresponding nonmalignant lung tissue ($p < 0.0001$).

FBN2 methylation with clinico-pathological features was also examined. There were no significant correlations in gender, age, smoking history (ever versus never smoked). The aberrant methylation of *FBN2* gene was present in 53% (49/92) cases of adenocarcinoma, and in 37% (11/30) of the squamous cell carcinoma cases. The difference between these results is not significant ($p = 0.09$). Because the number of squamous cell carcinomas and other histologies was small, we carried out a further study on the whole population of patients, unclassified by histology. The frequency of *FBN2* methylation was higher in the later T stages (T2, 3, 4) than in T1 ($p = 0.022$), higher in the later N stages (N1, 2, 3) than in N0 ($p = 0.037$), and in the later stages (II, III, IV) than in stage I ($p = 0.014$). However, *FBN2* methylation status did not correlate with survival ($p = 0.37$, log-rank test). The Cox proportional hazards model was also used to evaluate the effects of *FBN2* methylation with other explanatory variables on survival time, but the *FBN2* methylation was not a significant independent factor (data not shown).

4. Discussion

Tumor invasion is one of the earliest steps in the multistep process of metastasis and is characterized by cancer cells invading and breaking the basement membrane or other components of the extracellular matrix. Therefore, alteration of the extracellular matrix molecule is important for the development of malignant tumors [13]. FBN2, a large modular extracellular matrix glycoprotein found in many vertebrate organ systems, is known to be a key component of elastic fiber. Recently, Hagihara et al. demonstrated that *FBN2* is frequently methylated in pancreatic cancer [10]. However, there is no report on the role of FBN2 in lung cancer. To understand the role of *FBN2* gene in lung cancer, we examined the expression of *FBN2*. It was expressed in tracheal cells, and cultured airway epithelial cells, whereas the lung cancer cell lines showed a loss of 50% of the expression. Treatment with 5-Aza-CdR restored the expression of the gene in RT-PCR-negative cell lines, indicating that methylation is a major mechanism of transcriptional silencing of the gene. Also, tumor-specific methylation of *FBN2* gene was present in 49% of NSCLC. Although other mechanisms for disruption of the extracellular matrix exist, such as inactivation of laminin5-encoding genes [14–16] or overexpression of matrix metalloprotienases [17,18], aberrant methylation of *FBN2* may be one of those participating in the process of tumor progression.

In our study, two cell lines showed a loss FBN2 expression with a lack of aberrant methylation. This may have been due to other mechanisms of inactivating TSGs, such as loss of heterozygosity, point mutations, and homozygous deletions [19]. Also, we found FBN2 methylation in some of the matched nonmalignant lung tissues. Possible explanations for detecting methylated alleles in the nonmalignant lung tissues are that they may represent premalignant changes [20], or be related to age [21] or smoking [22].

In this study, 49% of *FBN2* methylation was associated with an increase in tumor size, lymph node involvement, and advanced stages. Although further study will be required in order to understand the role of FBN2 in the pathogenesis of advanced lung cancer, our data suggested that it is advantageous for tumor invasion and metastasis to downregulate *FBN2* gene of cancer cells. There are several reports about the correlation between the aberrant methylation of TSG and the progression of lung cancer [23,24]. *FBN2* may be added to the list of progression associated methylation genes of lung cancer because of the high frequency of methylation correlated significantly with progression. To

our knowledge, this is the first report that demonstrating the methylation of *FBN2* promoter in lung cancer and the correlation between *FBN2* methylation and lung cancer progression.

Our data did not show a significant association between *FBN2* methylation and patient survival. The lack of significance in the relationship of methylation to survival outcome may result from the limited number of patients taking part in our study, or on other factors.

In conclusion, we demonstrated frequent inactivation of *FBN2* gene through aberrant methylation of the promoter in NSCLC cell lines. We also found methylation of *FBN2* frequently in primary NSCLC; it correlated with the progression of the tumor from early to late stage disease. Aberrant methylation of *FBN2* gene appears to be an important factor in the pathogenesis of invasive NSCLC. Our findings of a frequent acquired tumor-related epigenetic alteration favor the candidacy of *FBN2* as a TSG.

Acknowledgements

This work was supported by a grant from Sasagawa Foundation Program. We thank Yusuke Suenaga, Biology Department, Faculty of Science, Chiba University, Japan for preparing cDNA. We greatly thank Dr. Toshikazu Ushijima, Chief, Carcinogenesis Division, National Cancer Center Research Institute, Japan for technical advice. We are also grateful to Mr. C.W. P. Reynolds for linguistic assistance with this manuscript.

References

[1] Shigematsu H, Suzuki M, Takahashi T, Miyajima K, Toyooka S, Shivapurkar N, et al. Aberrant methylation of HIN-1 (high in normal-1) is a frequent event in many human malignancies. Int J Cancer 2005;113(4):600–4.

[2] Sunaga N, Miyajima K, Suzuki M, Sato M, White MA, Ramirez RD, et al. Different roles for caveolin-1 in the development of non-small cell lung cancer versus small cell lung cancer. Cancer Res 2004;64(12):4277–85.

[3] Marsit CJ, Liu M, Nelson HH, Posner M, Suzuki M, Kelsey KT. Inactivation of the Fanconi anemia/BRCA pathway in lung and oral cancers: implications for treatment and survival. Oncogene 2004;23(4):1000–4.

[4] Gazdar AF, Miyajima K, Reddy J, Sathyanarayana UG, Shigematsu H, Suzuki M, et al. Molecular targets for cancer therapy and prevention. Chest 2004;125(5 Suppl.):97S–101S.

[5] Girard L, Zochbauer-Muller S, Virmani AK, Gazdar AF, Minna JD. Genome-wide allelotyping of lung cancer identifies new regions of allelic loss, differences between small cell lung cancer and non-small cell lung cancer, and loci clustering. Cancer Res 2000;60(17):4894–906.

[6] Suzuki M, Sunaga N, Shames DS, Toyooka S, Gazdar AF, Minna JD. RNA interference-mediated knockdown of DNA methyltransferase 1 leads to promoter demethylation and gene re-expression in human lung and breast cancer cells. Cancer Res 2004;64(9):3137–43.

[7] Toyooka S, Suzuki M, Tsuda T, Toyooka KO, Maruyama R, Tsukuda K, et al. Dose effect of smoking on aberrant methylation in non-small cell lung cancers. Int J Cancer 2004;110(3):462–4.

[8] Toyooka S, Suzuki M, Maruyama R, Toyooka KO, Tsukuda K, Fukuyama Y, et al. The relationship between aberrant methylation and survival in non-small-cell lung cancers. Br J Cancer 2004;91(4):771–4.

[9] Yang Q, Ota K, Tian Y, Kumar A, Wada J, Kashihara N, et al. Cloning of rat fibrillin-2 cDNA and its role in branching morphogenesis of embryonic lung. Dev Biol 1999;212(1):229–42.

[10] Hagihara A, Miyamoto K, Furuta J, Hiraoka N, Wakazono K, Seki S, et al. Identification of 27 5′ CpG islands aberrantly methylated and 13 genes silenced in human pancreatic cancers. Oncogene 2004;23(53):8705–10.

[11] Suzuki M, Shigematsu H, Takahashi T, Shivapurkar N, Sathyanarayana UG, Iizasa T, et al. Aberrant methylation of Reprimo in lung cancer. Lung Cancer 2005;47(3):309–14.

[12] Suzuki M, Toyooka S, Miyajima K, Iizasa T, Fujisawa T, Bekele NB, et al. Alterations in the mitochondrial displacement loop in lung cancers. Clin Cancer Res 2003;9(15):5636–41.

[13] Micke P, Tman A. A: Tumour-stroma interaction: cancer-associated fibroblasts as novel targets in anti-cancer therapy? Lung Cancer 2004;45(Suppl. 2):S163–75.

[14] Sathyanarayana UG, Maruyama R, Padar A, Suzuki M, Bondaruk J, Sagalowsky A, et al. Molecular detection of non-invasive and invasive bladder tumor tissues and exfoliated cells by aberrant promoter methylation of laminin-5 encoding genes. Cancer Res 2004;64(4):1425–30.

[15] Sathyanarayana UG, Padar A, Huang CX, Suzuki M, Shigematsu H, Bekele BN, et al. Aberrant promoter methylation and silencing of laminin-5-encoding genes in breast carcinoma. Clin Cancer Res 2003;9(17):6389–94.

[16] Sathyanarayana UG, Padar A, Suzuki M, Maruyama R, Shigematsu H, Hsieh JT, et al. Aberrant promoter methylation of laminin-5-encoding genes in prostate cancers and its relationship to clinicopathological features. Clin Cancer Res 2003;9(17):6395–400.

[17] Iizasa T, Fujisawa T, Suzuki M, Motohashi S, Yasufuku K, Yasukawa T, et al. Elevated levels of circulating plasma matrix metalloproteinase 9 in non-small cell lung cancer patients. Clin Cancer Res 1999;5(1):149–53.

[18] Suzuki M, Iizasa T, Fujisawa T, Baba M, Yamaguchi Y, Kimura H, et al. Expression of matrix metalloproteinases and tissue inhibitor of matrix metalloproteinases in non-small-cell lung cancer. Invas Metast 1998;18(3):134–41.

[19] Shapiro GI, Park JE, Edwards CD, Mao L, Merlo A, Sidransky D, et al. Multiple mechanisms of p16INK4A inactivation in non-small cell lung cancer cell lines. Cancer Res 1995;55(24):6200–9.

[20] Zochbauer-Muller S, Fong KM, Virmani AK, Geradts J, Gazdar AF, Minna JD. Aberrant promoter methylation of multiple genes in non-small cell lung cancers. Cancer Res 2001;61(1):249–55.

[21] Ahuja N, Issa JP. Aging, methylation and cancer. Histol Histopathol 2000;15(3):835–42.

[22] Vuillemenot BR, Pulling LC, Palmisano WA, Hutt JA, Belinsky SA. Carcinogen exposure differentially modulates RAR-beta promoter hypermethylation, an early and

frequent event in mouse lung carcinogenesis. Carcinogenesis 2004;25(4):623–9.

[23] Kim DH, Nelson HH, Wiencke JK, Christiani DC, Wain JC, Mark EJ, et al. Promoter methylation of DAP-kinase: association with advanced stage in non-small cell lung cancer. Oncogene 2001;20(14):1765–70.

[24] Seike M, Gemma A, Hosoya Y, Hemmi S, Taniguchi Y, Fukuda Y, et al. Increase in the frequency of p16INK4 gene inactivation by hypermethylation in lung cancer during the process of metastasis and its relation to the status of p53. Clin Cancer Res 2000;6(11):4307–13.

Oncogene (2006) 25, 1931–1942

www.nature.com/onc

ORIGINAL ARTICLE

Increased expression of proapoptotic *BMCC1*, a novel gene with the *BNIP2* and *Cdc42GAP* homology (BCH) domain, is associated with favorable prognosis in human neuroblastomas

T Machida[1,2,5], T Fujita[1,2,5], ML Ooo[1], M Ohira[1], E Isogai[1], M Mihara[1,2], J Hirato[3], D Tomotsune[1], T Hirata[4], M Fujimori[2], W Adachi[2] and A Nakagawara[1]

[1]*Division of Biochemistry, Chiba Cancer Center Research Institute, Chiba, Japan;* [2]*Department of Surgery, Shinshu University School of Medicine, Matsumoto, Nagano, Japan;* [3]*Department of Pathology, Gunma University School of Medicine, Maebashi, Gunma, Japan and* [4]*Hisamitsu Pharmaceutical Co. Inc., Tokyo, Japan*

Differential screening of the genes obtained from cDNA libraries of primary neuroblastomas (NBLs) between the favorable and unfavorable subsets has identified a novel gene *B*CH *m*otif-containing molecule at the *c*arboxyl terminal region *1* (*BMCC1*). Its 350 kDa protein product possessed a Bcl2-/adenovirus E1B nineteen kDa-interacting protein 2 (BNIP2) and Cdc42GAP homology domain in the COOH-terminus in addition to P-loop and a coiled-coil region near the NH_2-terminus. High levels of *BMCC1* expression were detected in the human nervous system as well as spinal cord, brain and dorsal root ganglion in mouse embryo. The immunohistochemical study revealed that BMCC1 was positively stained in the cytoplasm of favorable NBL cells but not in unfavorable ones with *MYCN* amplification. The quantitative real-time reverse transcription–PCR using 98 primary NBLs showed that high expression of *BMCC1* was a significant indicator of favorable NBL. In primary culture of newborn mice superior cervical ganglion (SCG) neurons, m*BMCC1* expression was downregulated after nerve growth factor (NGF)-induced differentiation, and upregulated during the NGF-depletion-induced apoptosis. Furthermore, the proapoptotic function of BMCC1 was also suggested by increased expression in CHP134 NBL cells undergoing apoptosis after treatment with retinoic acid, and by an enhanced apoptosis after depletion of NGF in the SCG neurons obtained from newborn mice transgenic with *BMCC1* in primary culture. Thus, BMCC1 is a new member of prognostic factors for NBL and may play an important role in regulating differentiation, survival and aggressiveness of the tumor cells.
Oncogene (2006) **25,** 1931–1942. doi:10.1038/sj.onc.1209225; published online 14 November 2005

Keywords: BMCC1; neuroblastoma; apoptosis; BNIP2; Cdc42GAP; BCH domain

Correspondence: Dr A Nakagawara, Division of Biochemistry, Chiba Cancer Center Research Institute, 666-2 Nitona, Chuoh-ku, Chiba 260-8717, Japan.
E-mail: akiranak@chiba-cc.jp
[5]These authors contributed equally to this work.
Received 13 April 2005; revised 15 September 2005; accepted 29 September 2005; published online 14 November 2005

Introduction

Neuroblastoma (NBL) is one of the most common pediatric neoplasms and originates from the sympathoadrenal lineage of neural crest. However, its biological as well as clinical behavior is highly heterogeneous. The tumors occurred in the patients under 1 year of age have a tendency to spontaneously regress or differentiate (Evans *et al.*, 1976). On the other hand, the tumors found in the patients more than 1 year of age are usually aggressive and often kill the patients. The latter subsets of the tumor frequently have multiple genomic aberrations which include frequent loss of the distal part of the short arm of chromosome 1, amplification of the *MYCN* oncogene, and gain of chromosome 17q, all of which are associated with unfavorable prognosis (Brodeur *et al.*, 1984; Caron, 1995).

Although the molecular mechanism underlying regression of NBL is still unclear, accumulating evidence suggests that the signals from neurotrophic factors and their receptors play an important role in regulating growth, differentiation and programmed cell death. High expression of *TrkA*, a high affinity receptor for nerve growth factor (NGF), is associated with the favorable outcome, and there is an inverse correlation between *TrkA* expression and *MYCN* amplification. Cells expressing functional TrkA may be susceptible to either programmed cell death leading to tumor regression, especially in infants, or to differentiation to a benign ganglioneuroma. Thus, like normal sympathetic neurons, a limited amount of NGF may be supplied from the stromal cells such as Schwann cells and fibroblasts, that at least partly regulates differentiation and programmed cell death of the NBL cells. In contrast, TrkB, another family member, is preferentially expressed in aggressive NBL cells together with its preferred ligands BDNF and NT-4/5 which stimulate proliferation in an autocrine/paracrine manner, conferring potency to invade and/or metastasize on the tumor cells (Nakagawara *et al.*, 1993, 1994).

The proto-oncogene *bcl-2* encodes a 25-kDa mitochondrial membrane protein that inhibits programmed cell death (Hockenbery *et al.*, 1990; Garcia *et al.*, 1992;

Oltvai *et al*., 1993). The recent reports have suggested that *bcl-2* protein is expressed at relatively high levels in both NBLs and neural crest cells. However, the role of *bcl-2* in the regulation of differentiation and survival of NBL cells is still elusive.

In order to clarify the molecular mechanism of cellular signaling related to regression of NBL, we have cloned a large number of genes from full-length-enriched oligo-capping cDNA libraries constructed from two different subsets of NBL with favorable and unfavorable biology (Ohira *et al*., 2003a, b). Sequence analysis of the genes from those libraries has revealed that the expression profile is significantly different between the both subsets. Screening by using semiquantitative RT–PCR has shown that more than 500 genes are differentially expressed between them. In the present paper, we report cloning and functional characterization of a novel gene termed as *B*cl2-/adenovirus E1B *n*ineteen kDa-*i*nteracting *p*rotein *2* (*B*NIP2) and *Cdc42GAP* homology *B*CH *m*otif-containing molecule at the *c*arboxyl terminal region *1* (*BMCC1*), which is preferably expressed in favorable NBL.

Results

Full-length cDNA cloning and structural analysis of the BMCC1 *gene*

As reported previously, we constructed oligo-capping cDNA libraries from different subsets of primary NBLs (Ohira *et al*., 2003b). After DNA sequencing both ends of about 10 000 clones randomly picked up, we obtained 5000 independent genes, among which about 2000 were found to be novel by homology search. They were then subjected to semi-quantitative RT–PCR to examine if they are differentially expressed between favorable (stage 1, less than 1-year-old, single copy of *MYCN* and high expression of *TrkA*) and unfavorable (stage 3 or 4, more than 1-year-old, amplified *MYCN* and low expression of *TrkA*) subsets of NBL. The differential screening in a panel of template cDNAs obtained from 16 favorable and 16 unfavorable primary NBLs demonstrated an interesting novel gene (*Nbla00219*) which had a BNIP2 and BCH domain, a recently reported new motif which might interact with Bcl-2 protein, at the COOH-terminus. It was preferentially expressed in favorable NBLs.

Sequencing of the *Nbla00219* clone showed that the insert size was 2277 bp with a putative open reading frame (ORF) of 1452 bp (484 amino acids) localized at the 5′-end region. The database search demonstrated that the *Nbla00219* sequence matched to the *KIAA0367* cDNA (accession no.: AB002365) with 95% identity as well as a part of the genomic sequence within the BAC clone RP11-146P9 (GenBank accession no.: AL161625) which was mapped to chromosome 9p13. However, there was no in-frame stop codon in the upstream region of the putative initiation site of *KIAA0367*, suggesting that the coding region of the gene extended over the 5′-end. In fact, Northern blot analysis of human fetal brain mRNA using *nbla00219* cDNA as a probe demonstrated that the transcript size was approximately 12 kb (Figure 1d). In order to determine a full-length cDNA of this gene, we performed gene prediction according to the sequence information from the BAC clone RP11-146P9 by using several algorithm. The exons expected in the upstream region of the gene were confirmed by RT–PCR using cDNA libraries constructed from human fetal brain and/or NBL tissues with favorable prognosis as template with subsequent DNA sequencing. It revealed that the gene contained a large exon of about 6.5 kb within the extended 5′-coding region. The predicted 5′-side ORF was also confirmed by matching to the several mouse ESTs. Then, we finally identified the full-length *Nbla00219* cDNA (Figure 1a) with a 5′-untranslated region of 323 bp (nt. no. 1-323), an ORF of 8355 bp (nt. no. 324-8497), and a 3′-untranslated region of 3196 bp (nt. no. 8498-11 690) (accession no.: AB050197). The Kozak consensus sequence for translation initiation site (Kozak, 1987) was found at the putative ATG start codon (at position 324), though no in-frame stop codon was found in the upstream region. The blast search against public databases showed no significant homology except BNIP2 (accession no.: XM007602, 52% identity) and Cdc42GAP (accession no.: NM004308, 38% identity) at the COOH-terminal end of the full-length *Nbla00219* (Figure 1a and b). Since the region had been termed as the BCH domain which was highly conserved among the three genes (Figure 1c), we named the full-length *Nbla00219* gene as *BMCC1*.

The BCH domain acts as the GTPase activating protein (GAP) in BNIP2. There are two critical arginine residues, Arg-236 and Arg-238, which are important for conferring the GAP activity to the Cdc42 homodimers (Zhang and Zheng, 1998; Zhang *et al*., 1999; Low *et al*., 2000). In BMCC1, both critical arginine residues were well conserved. Using several algorithms to predict the secondary structure of amino acids and the intracellular localization, we found the coiled-coil motif (amino acids 918–941) and P-loop (amino acids 2293–2300) within the BMCC1 protein (Figure 1a). Three putative transmembrane domains (amino acids 2545–2563, 2573–2597 and 2632–2653) were also suggested.

Although *BMCC1* was expressed significantly at higher levels in favorable than unfavorable NBLs, the expression levels of *BNIP2 family* were similar between the NBL subsets (Figure 2a).

Expression of BMCC1 *in human tissues and cell lines*

To study the expression pattern of *BMCC1* mRNA in human tissues, we performed semiquantitative RT–PCR. *BMCC1* was expressed in many tissues examined except for bone marrow, thymus and spleen (Figure 2c). The high levels of expression were seen in the nervous system (brain, cerebellum and spinal cord) as well as adrenal gland which were the tissues NBL originated from. We further performed semiquantitative RT–PCR to examine the expression levels of *BMCC1* in cultured cell lines including NBL and other cancers. *BMCC1* was expressed in most of 17 NBL cell lines tested (Figure 2b). Among the other cancer lines, high expression of *BMCC1* was observed in rhabdomyosar-

a

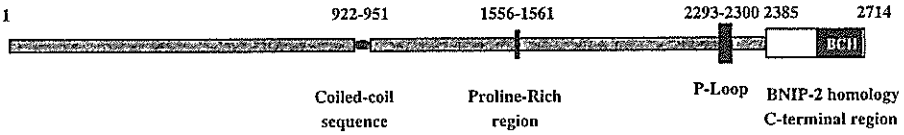

b

```
MVSNSRTSSTEAVAGSAPLSQGSSGIMELYGSDIEPQPSSVNFIENPPDLNDSNQAQVDANVDLVSPDSGLATIRSSRSSKESSVFLSDDSPVGEGAGPH 100
HTLLPGLDSYSPIPEGAVAEEHAWSGEHGEHFDLFNFDPAPMASGQSQQSSHSADYSPADDFFPNSDLSEGQLPAGPEGLDGMGTNMSNYSSSSLLSGAG 200
KDSLVEHDEEFVQRQDSPRDNSERNLSLTDFVGDESPSPERLKNTGKRIPPTPMNSLVESSPSTEEPASLYTEDTTQKATDTGHMGPPQTHARRSSWWGG 300
LEIDSKNIADAWSSSEQESVFQSPESWKEHKPSSIDRRASDSVFQPKSLEFTKSGPWESEFGQPELGSNDIQDKNEESLPFQNLPMEKSPLPNTSPQGTN 400
HLIEDFASLWHSGRSPTAMPEPWGNPTDDGEPAAVAPFPAWSAFGKEDHDEALKNTWDLHPTSSKTPSVRDPNEWAMAKSGFAFSSSELLDNSPSEINNE 500
AAPEIWGKKNNDSRDHIFAPGNPSSDLDHTWTNSKPPKEDQNGLVDPKTRGKVYEKVDSWNLFEENMKKGGSDVLVPWEDSFLSYKCSDYSASNLGEDSV 600
PSPLDTNYSTSDSYTSPTFAGDEKETEHKPFAKEEGFESKDGNSMAEETDIPPQSLQQSLQQSSRNRISSGPGNLDMWASPHTDNSSEINTTHNLDENEL 700
KTEHTDGKNISMEDDVGESSQSSYDDPSMMQLYNETNRQLTLLHSSTNSRQTAPDSLDLWNRVILEDTQSTATISDMDNDLDWDDCSGGAAIPSDGQTEG 800
YMAEGSEPETRFTVRQLEPWGLEYQEANQVDWELPASDEHTKDSAPSEHHTLNEKSGQLIANSIWDSVMRDKDMSSFMLPGSSHITDSEQRELPPEIPSH 900
SANVKDTHSPDAPAASGTSESEALISHLDKQDTERETLQSDAASLATRLENPGYFPHPDPRKGHGDGQSESEKEAQGATDRGHLDEEEVIASGVENASGI 1000
SEKGQSDQELSSLVASEHQEICIKSGKISSLAVTFSPQTEEPEEVLEYEEGSYNLDSRDVQTGMSADNLQPKDTHEKHLMSQRNSGETTETSDGMNFTKY 1100
VSVPEKDLEKTEECNFLEPENVGGGPPHRVPRSLDFGDVPIDSDVHVSNTRSEITKNLDVKGSENSLPGAGSSGNFDRDTISSEYTHSSASSPELNDSSV 1200
ALSSWGQQPSSGYQEENQGNWSEQNHQESELITTDGQVEIVTKVKDLEKNRINEFEKSFDRKTPTFLEIWNDSVDGDSFSSLSSPETGKYSEHSGTHQES 1300
NLIASYQEKNEHDISATVQPEDARVISTSSGSDDDSVGGEESIEEEIQVANCNVAEDESRAWDSLNESNEFLVTADPKSENIYDYLDSSEPAENENKSNP 1400
FCDNQQSSPDPWTFSPLTETEMQITAVEKEKRSSPETGTTGDVAWQISPKASFPKNEDNSQLEMLGFSADSTEWWTSPQEGRLIESPFERELSDSSGVLE 1500
INSSVHQNASPWGVPVQGDIEPVETHYTNPFSDNHQSPFLEGNGKNSHEQLWNIQPRQPDPDADKFSQLVKLDQIKEKDSREQTFVSAAGDELTPETPTQ 1600
EQCQDTMLPVCDHPDAAFTHAEENSCVTSNVSTNEGQETNQWEQEKSYLGEMTNSSIATENFPAVSSPTQLIMKPGSEWDGSTPSEDSRGTFVPDILHGN 1700
FQEGGQLASAAPDLWMDAKKPFSLKADGENPDILTHCEHDSNSQASDSPDICHDSEAREETEKHLSACMGPEVESSELCLTEPEIDEEPIYEPGREFVPS 1800
NAELDSENATVLPPIGYQADIKGSSQPTSHKGSPEPSEINGDNSTGLQVSEKGASPDMAPILEPVDRRIPRIENVATSIFVTHQEPTPEGDGSWISDSFS 1900
PESQPGARALFDGDPHLSTENPALVPDALLASDTCLDISEAAFDHSFSDASGLNTSTGTIDDMSKLTLSEGHPETPVDGDLGKQDICSSEASWGDFEYDV 2000
MGQNIDEDFLREPEHFLYGGDPPLEEDSLKQSLAPYTPPFDLSYLTEPAQSAETIEEAGSPEDESLGCRAAEIVLSALPDRRSEGNQAETKNRLPGSQLA 2100
VLHIREDPESVYLPVGAGSNILSPSNVDWEVETDNSDLPAGGDIGPPNGASKEIPELEEEKTIPTKEPEQIKSEYKEERCTEKNEDRHALHMDYILVNRE 2200
ENSHSKPETCEERESIAELELYVGSKETGLQGTQLASFPDTCQPASLNERKGLSAEKMSSKGDTRSSFESPAQDQSWMFLGHSEVGDPSLDARDSGPGWS 2300
GKTVEPFSELGLGEGPQPQILEEMKPLESLALEEASGPVSQSQKSKSRGRAGPDAVTHDNEWEMLSPQPVQKTMIPDTEMEEETEFLELGTRISRPNGLL 2400
SEDVGMDIPFEEGVLSPSAADMRPEPPNSLDLNDTHPRRIKLTAPNINLSLDQSEGSILSDDNLDSPDEIDINVDELDTPDEADSFEYTGHDPTANKDSG 2500
QESESIPEYTAEEEREDNRLWRTVVIGEQEQRIDMKVIEPYRRVISHGGYYGDGLNAIIVFAACFLPDSSRADYHYVMENLFLYVISTLELMVAEDYMIV 2600
YLNGATPRRRMPGLGWMKKCYQMIDRRLRKNLKSFIIVHPSWFIRTILAVTRPFISSKFSSKIKYVNSLPELSGLIPMDCIHIPESIIKTSCLYNDPEMS 2700
SMEKDIDLKLKEKP 2714
```

c

```
BMCC1       2542:RRVISHGG------YYGDGLNAIIVFAACFLPDSSRADYHYVMENLFLYVISTLE LMVAEDYMIVYLNGATPRRRMPGLGWMKKCYQMI
BNIP2        151:KKVISHGG------YYGDGLNAIVVFAVCFMPESSQPNYRYLMDNLFKYVIGTLE LLVAENYMIVYLNGATTRRKMPSLGWLRKCYQQI
BNIP-Salpha  117:KKVLSHGG------YHGDGLNAVILFASCYLPRSSIPNYTYVMEHLFRYMVGTLE LLVAENYLLVHLSGGTSRAQVPPLSWIRQCYRTL
BNIP-Sbeta   117:KKVLSHGG------YHGDGLNAVILFASCYLPRSSIPNYTYVMEHLFRYMVGTLE LLVAENYLLVHLSGGTSRAQVPPLSWIRQCYRTL
Cdc42GAP     85:----------------------IIVFSACRMPPSHQLDHSKLLG----YLKHTLD QYVESDYTLLYLHHGLTSDNKPSLSWLRDAYREF

BMCC1       2646:DRRLRKNLKSFIIVHPSWFIRTILAVTRPFISSKFSSKIKYVNSLPELSGLIPMDCIHIPESIIKTSCLYNDPEMS SMEKDIDLKLKEKP 2714 (100%)
BNIP2        234:DRRLRKNLKSLIIVHPSWFIRTLLAVTRPFISSKFSQKIRYVFNLAELAELVPMEYVGIPECI-KQVDQELNG-KQ DEPKNEQ------- 314  (57%)
BNIP-Salpha  200:DRRLRKNLRALVVVHATWYVKAFLALLRPFISSKFTRKIRFLDSLGELAQLISLDQVHIPEAVRQLDRDLHGSGGT ---------- 275  (41%)
BNIP-Sbeta   200:DRRVL---------- ---------- 204  (42%)
Cdc42GAP     148:DRKYKKNIKALYIVHPTMFIKTLLILFKPLISPKFGQKIFYVNYLSELSEHVKLEQLGIPRQVLK----YDDFLKS TQKSP--------- 224  (34%)
```

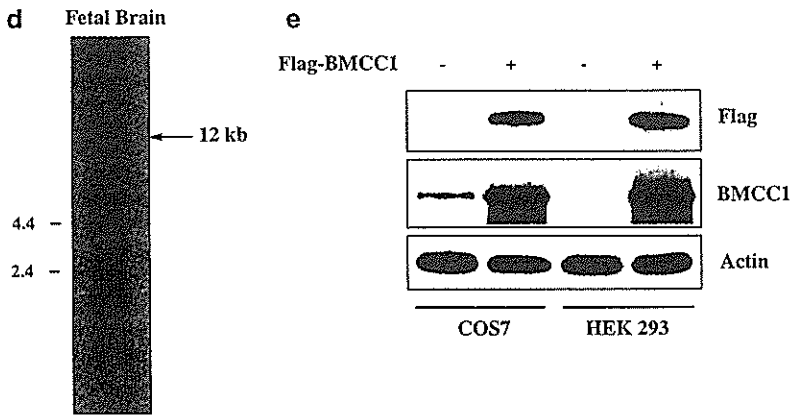

Figure 1 Molecular cloning of BMCC1. (a) Schematic structure of BMCC1. BMCC1 contains coiled-coil sequence, proline-rich region, P-loop and BCH domain in its concurrent position. (b) Full-length amino-acid sequence of human BMCC1. Coiled-coil, proline-rich and P-loop regions were underlined and BCH domain was indicated in box. (c) Alignment of C-terminal regions of BMCC1, BNIP-2, BNIP-Salpha, BNIP-Sbeta, and Cdc42GAP homologous to BCH domain. Total number of amino-acid residues of each protein and their percent homology were described at the end of each sequence. RRKMP (homophilic/heterophilic dimerized sequence), EYV (binding to switch I and insert region of Cdc42) (Low *et al*., 2000) and RRLRK (arginine patch of BCH domain), ATWYVKA (binding motif for homophilic complex and critical for proapoptotic activity) (Zhou *et al*., 2002), were underlined. (d) Northern blot analysis of *BMCC1* transcript in fetal brain tissue. Total RNA (25 μg) purchased from Clontech was loaded for Northern blotting. Left; size markers showing 2.4 and 4.4 kb. (e) BMCC1 expression in COS7 and HEK293 cells. pCAGGS-BMCC1-Flag was transfected into COS7 and HEK 293 cells and lysed after 48 h. Cell lysates were run into 8% SDS–PAGE in 35 mA for more than 4 h, transferred to immobilon-P membrane (MILLIPORE) and probed by anti-Flag, anti-BMCC1 (C-terminal end epitope), and antiactin antibodies.